

# Photoelectric Emission from Interstellar Dust: Grain Charging and Gas Heating

Joseph C. Weingartner

Physics Dept., Jadwin Hall, Princeton University, Princeton, NJ 08544, USA; CITA, 60 St. George Street, University of Toronto, Toronto, ON M5S 3H8, Canada;  
weingart@cita.utoronto.ca

and

B.T. Draine

Princeton University Observatory, Peyton Hall, Princeton, NJ 08544, USA;  
draine@astro.princeton.edu

## ABSTRACT

We model the photoelectric emission from and charging of interstellar dust and obtain photoelectric gas heating efficiencies as a function of grain size and the relevant ambient conditions, which affect the grain charging. We also construct grain size distributions for which there is substantial mass in very small graphite grains and which are consistent with the observed average extinction for lines of sight with  $R_V = 3.1, 4.0,$  and  $5.5$ . We evaluate the net gas heating rate for each of these size distributions, and find less heating (by as much as an order of magnitude) for dense regions characterized by  $R_V = 5.5$  than for diffuse regions with  $R_V = 3.1$ . We provide fitting functions which reproduce our numerical results for photoelectric heating and recombination cooling for a wide range of interstellar conditions. In a separate paper we will examine the implications of these results for the thermal structure of the interstellar medium. Finally, we investigate the potential importance of photoelectric heating in H II regions, including the warm ionized medium. We find that photoelectric heating could be comparable to or exceed heating due photoionization of H for high ratios of the radiation intensity to the gas density.

*Subject headings:* dust — extinction — HII regions — ISM: clouds

## 1. Introduction

Photoelectric emission from dust grains dominates the heating of diffuse interstellar gas clouds as well as the photodissociation regions at the surfaces of molecular clouds. This mechanism therefore plays an important role in the dynamical evolution of the interstellar medium, and in shaping the line emission spectra of galaxies. Heating by photoelectric emission from interstellar grains was first considered by Spitzer (1948), and there have since been a number of reassessments of the heating rate (Watson 1972; deJong 1977; Draine 1978; Tielens & Hollenbach 1985; Bakes & Tielens 1994, Dwek & Smith 1996).

For a given grain, the heating rate depends on the grain size, composition, and charge state, as well as on the spectrum of the illuminating radiation. Because photoelectric yields are enhanced for small grains (Watson 1972, 1973), estimates of the net photoelectric heating rate in interstellar gas are sensitive to the adopted grain size distribution, which should be consistent with the observed extinction curve (which shows strong regional variations) as well as with the observed emission from interstellar dust grains, from the near-infrared to the microwave. Previous estimates for photoelectric heating rates did not always use grain size distributions which were consistent with these constraints. While the measured extinction curve by itself does not suffice to uniquely specify the grain size distribution, in the present study we will consider size distributions which are consistent with the observed extinction in different regions, with either the minimum or maximum permissible population of ultrasmall grains.<sup>1</sup>

In addition to using size distributions consistent with observations, we also model the photoelectric emission process and associated grain charging in detail, using realistic yields for graphitic and silicate grains, a realistic distribution of photoelectron kinetic energies, and new estimates for electron sticking efficiencies for small grains. The resulting photoelectric heating rates are calculated for grain size distributions consistent with extinction curves characteristic of diffuse clouds ( $R_V \equiv A_V/E_{B-V} \approx 3.1$ ), intermediate density regions ( $R_V \approx 4.0$ ), and dense clouds ( $R_V \approx 5.5$ ).

---

<sup>1</sup>These small “grains” are actually large molecules (as are all grains). We do not yet know which molecules are present; polycyclic aromatic hydrocarbons are inferred from infrared emission features (Léger & Puget 1984, Sellgren 1994), but we cannot yet specify which particular species are present in the ISM. Absent knowledge of the physical properties of the large carbonaceous molecules, we categorize them with their larger relatives, the grains. In particular, we assume that their optical and ultraviolet optical properties are the same as for graphite. Also, as detailed in §2, we assume that the ionization potential and photoelectric yield vary continuously with size for the entire carbonaceous grain population. Once the identity and physical properties of the large carbonaceous molecules have been determined, this simplifying approach of labelling large molecules as very small grains can be superseded.

In §2 we discuss our adopted model for photoelectric emission from grains, expanding on the treatments of Draine (1978) and Bakes & Tielens (1994). In §3 we use recent experimental results to obtain improved estimates for the electron sticking coefficient, as a function of grain size; our new sticking coefficients differ significantly from previous estimates. In §4 we characterize the relevant ambient conditions (which are important in grain charging) and in §5 we evaluate the photoelectric heating efficiency as a function of grain size. In §6 we obtain several grain size distributions, with various fractions of the total grain mass in very small grains, which reproduce the average observed extinction for lines of sight with  $R_V = 3.1, 4.0,$  and  $5.5$ . We obtain net heating rates in H I regions for some of these distributions in §7, and investigate the potential contribution of photoelectric heating in H II regions in §8. We briefly summarize our results in §9.

## 2. Photoelectric Emission from Grains

### 2.1. Grain Geometry

While recognizing that interstellar grains are generally nonspherical, we will characterize each grain by an effective radius  $a$ , the radius of a sphere of equal volume. Ideal graphite has density  $\rho = 2.25 \text{ g cm}^{-3}$ , but pyrolytic graphite, glassy carbon, and amorphous carbon have lower densities, so for carbonaceous grains we will assume that the carbon atoms contribute a mass density  $1.5 \text{ g cm}^{-3}$ . Thus, the number  $N_C$  of carbon atoms in a carbonaceous grain is taken to be related to the radius  $a$  through

$$N_C = 314 \left( \frac{a}{10^{-7} \text{ cm}} \right)^3 . \quad (1)$$

For example, coronene  $\text{C}_{24}\text{H}_{12}$  is assigned an effective radius  $a = 4.2 \text{ \AA}$ , and a surface area  $4\pi a^2 = 230 \text{ \AA}^2$ .

In following sections, the  $N_C$ - $a$  relation will be used to incorporate experimental data on hydrocarbon molecules into our description in terms of the effective radius. We also consider photoemission from silicate grains, but since small molecules that extrapolate to silicates as  $a \rightarrow \infty$  have not been studied, we will not need a similar relation for silicates.

### 2.2. Electron Energy Levels

The electrons in a solid are confined in a potential well (see, e.g., Lang & Kohn 1971). For neutral bulk material, the work function  $W$  is the energy of a free electron with zero

kinetic energy minus the energy of an electron in the highest occupied state in the solid. (Throughout this section, refer to Figure 1 for schematic depictions of the electron-confining potential.) In this case, the ionization potential  $IP$ , i.e. the energy required to liberate an electron from the highest occupied state to infinity, equals  $W$ .

For small grains,  $IP \neq W$ . We first consider grains which are not so small that quantum effects shift the energy levels from their bulk values. If  $Z \geq 0$ , then an electron that is liberated from the grain material feels a Coulomb attraction to the grain, which now has charge  $(Z + 1)e$ . For a conducting sphere,  $IP - W$  can be determined by calculating the work needed to remove the electron from a point just outside the sphere to infinity (including the term due to the image charge as well as that due to the net charge on the sphere) and subtracting the corresponding work associated with a plane surface. The result is that  $IP = W + (Z + 1/2)e^2/a$  (see, e.g. Makov, Nitzan, & Brus 1988; Seidl & Brack 1996).<sup>2</sup> For arbitrary materials, the second term above should be multiplied by  $(\epsilon - 1)/\epsilon$ , where  $\epsilon$  is the dielectric function (Makov et al. 1988). This correction is fairly small for candidate grain materials, so we will ignore it.

Of course, we cannot calculate the quantum shifts for very small grains. Instead, we adopt an empirical approach. Figure 2 shows the first and second ionization potentials  $IP(0)$  and  $IP(1)$  for various aromatic hydrocarbons, including  $C_6H_6$  benzene,  $C_{24}H_{12}$  coronene, and  $C_{38}H_{20}$  benz[42]. The polycyclic aromatic hydrocarbons (PAHs) of interest here appear to be fit by

$$IP(Z) = W + \left(Z + \frac{1}{2}\right) \frac{e^2}{a} + (Z + 2) \frac{e^2}{a} \left(\frac{0.6 \text{ \AA}}{a}\right) \quad , \quad (2)$$

with the graphite work function  $W = 4.4 \text{ eV}$ . This estimate for  $IP(Z)$  is plotted in Figure 2 for  $Z = 0$  and 1. For the first ionization potential  $IP(0)$ , equation (2) is numerically very close to the estimate of Bakes (1992) and Bakes and Tielens (1994), but for  $IP(1)$  our estimate is  $\sim 1 \text{ eV}$  below their estimate for PAHs with  $\sim 15\text{-}30 \text{ C}$  atoms. Note that equation (2) reproduces the classical electrostatic result for large  $a$ .

For silicates, few laboratory experiments are available to guide us. We adopt  $W = 8 \text{ eV}$ , since the photoelectric yield for lunar dust drops steeply around that energy (Feuerbacher et al. 1972). Nayak et al. (1998) have made theoretical calculations of the ionization potentials of small silica clusters  $(SiO_2)_n$ , with  $n = 1$  to 6. They find  $IP = 11.19 \text{ eV}$  ( $16.08 \text{ eV}$ ) for  $n = 2$  (5), and intermediate results for other values of  $n$ . If we employ

---

<sup>2</sup>Surprisingly, there has been some controversy in the literature as to the value of the constant added to  $Z$ . See Makov et al. (1988), Moskovits (1991), Seidl & Brack (1996).

equation (2) with  $W = 8 \text{ eV}$  and  $a \approx 3.2 \text{ \AA}$ , then we find  $IP \approx 12 \text{ eV}$ , which is in the Nayak et al. range for small clusters. Thus, we adopt equation (2) for both carbonaceous and silicate grains, with  $W = 4.4$  and  $8 \text{ eV}$ , respectively.

We assume that, when  $Z > 0$ , the highest occupied energy level is very close to the top of the valence band, since the number of electrons which have been removed from the grain is small compared with the total number of electrons in the grain. Thus, for  $Z \geq 0$ , the threshold photon energy for photoelectric emission is given by  $h\nu_{\text{pet}}(Z) = IP(Z)$ .

The description of a negatively charged grain differs from that of a positively charged or neutral grain in two major respects. First, the repulsive Coulomb potential presents the opportunity for electrons to tunnel out of the grain (when  $Z < -1$ ). Second, if the valence band is full in the neutral grain, then the “extra” electrons, which occupy the “LUMO” (for “lowest unoccupied molecular orbital” of the neutral), are separated from the top of the valence band by the band gap, with extra energy  $E_{\text{bg}}$ . The electron affinity  $EA(Z)$  is the difference in energy between infinity and the LUMO for the grain of charge  $(Z - 1)e$  created by adding the electron. Suppose the tunneling probability becomes significant when the electron energy exceeds the potential at infinity by  $E_{\text{min}}$ . The threshold photon energy for photodetachment from a grain with charge  $Ze$ , in which an “attached” electron in the LUMO is removed, is given by  $h\nu_{\text{pdt}}(Z) = E_{\text{min}} + EA(Z + 1)$ .<sup>3</sup> Likewise, the threshold for photoelectric emission (i.e. emission of an electron from the valence band) is  $h\nu_{\text{pet}}(Z) = E_{\text{min}} + EA(Z + 1) + E_{\text{bg}}$ .

From Figure 1 we expect that

$$EA(Z \leq 0) = W - E_{\text{bg}}(a) + \left( Z - 1 + \frac{1}{2} \right) \frac{e^2}{a} + O(a^{-2}) \quad , \quad (3)$$

where the presence of an  $O(a^{-2})$  term is expected since such a correction was required to fit the experimental results for  $IP(Z \geq 0)$  (eq. 2). The “infinite limit” for PAHs – graphite – is a “semimetal”, with a slight overlap between the top of the valence band and the conduction band (Spain 1973). For metals and semimetals,  $E_{\text{bg}} = 0$ . Many silicates begin to absorb strongly around 2500–2000  $\text{\AA}$ , corresponding to a band gap of 5–6 eV; we will adopt  $E_{\text{bg}} = 5 \text{ eV}$ , independent of  $a$ , for silicates.

Values of  $EA(0)$  are shown in Figure 3 for selected neutral PAHs, benzene, and  $\text{C}_{60}$ . The relation

$$EA(Z) = W + \left( Z - \frac{1}{2} \right) \frac{e^2}{a} - \frac{e^2}{a} \left( \frac{5 \text{ \AA}}{a + 6 \text{ \AA}} \right) \quad (4)$$

---

<sup>3</sup>Here we ignore the possibility that photodetachment leaves the grain in a vibrationally excited state.

is also plotted in Figure 3, for  $Z = 0$  and  $W = 4.4 \text{ eV}$ . For  $a \rightarrow \infty$  this has the theoretically expected behavior, and it provides a reasonable fit to the experimental values of  $EA(0)$  for benzene and the PAHs in Figure 3 (for which  $a \approx 2.7 - 6 \text{ \AA}$ ). We adopt this equation (4) for carbonaceous grains. For silicates, we adopt

$$EA(Z) = W - E_{\text{bg}} + \left( Z - \frac{1}{2} \right) \frac{e^2}{a}, \quad (5)$$

with  $W - E_{\text{bg}} = 3 \text{ eV}$ . This yields  $EA(0) \approx 0.73 \text{ eV}$  for  $a \approx 3.2 \text{ \AA}$ , which is somewhat low compared with the values of 2–3 eV inferred for small silica clusters (Wang et al. 1997).

### 2.3. Photoelectric Yields

The photoelectric yield is the probability that an electron will be ejected following the absorption of a photon. Of course, we cannot calculate the yield from first principles. Draine (1978) displayed yield measurements from experiments on bulk samples of materials of interest, including graphite, lunar dust, and silicon carbide. Watson (1972, 1973) pointed out that the yields of submicron particles are expected to be enhanced relative to the bulk yields, because of the finite electron escape length. An electron excited somewhere in the volume of the sample can lose energy during its journey to the surface, through interactions with electrons and with phonons. The result is that the fraction of electrons which escape energy loss goes roughly as  $\exp(-x/l_e)$ , where  $x$  is the distance the electron has traveled and  $l_e$  is the “electron escape length.” Generally, the photon attenuation length,  $l_a$  (equal to the  $e$ -folding length for the decrease in radiation intensity as it propagates into the material), exceeds  $l_e$ , and the electrons excited deep inside a bulk sample do not reach the surface. Small grain sizes limit the distance from electron excitation to surface, so the yield is enhanced.

A detailed and accurate model for the above geometrical effect is not yet available. A series of experiments (Schmidt-Ott et al. 1980; Burtscher & Schmidt-Ott 1982; Burtscher et al. 1984; Müller et al. 1988) on free silver spheres with radii between 27 and 54  $\text{\AA}$  found yield enhancements in excess of expectations by factors of several. A later theoretical effort (Faraci, Pennisi, & Margaritondo 1989) was able to reproduce the results, but only by assuming that the condition for an electron to escape, when incident on the surface from within, depends only on its energy and not on its direction of motion. The estimates adopted here for size-dependent yields from grains are based on Watson’s (1973) simplified model for the geometrical effect and must be regarded as provisional. Reliable calculations of effects involving photoelectric emission from interstellar dust will not be possible until experiments have been performed on submicron grains of appropriate composition.

For negatively charged grains we will distinguish between “photoelectric” ejection of electrons from the valence band and “photodetachment” of excess “attached” electrons.

### 2.3.1. Valence Band Electrons

For the valence band electrons, we assume that photoelectric emission requires  $\nu > \nu_{\text{pet}}$ , where the photoelectric threshold energy

$$h\nu_{\text{pet}}(Z, a) = \begin{cases} IP(Z, a) & , Z \geq 0 \\ W + \left(Z + \frac{1}{2}\right) e^2/a + E_{\text{min}}(Z, a) & , Z < 0 \end{cases} ; \quad (6)$$

$E_{\text{min}}(Z, a)$  is the electron energy (with respect to the potential at infinity) above which excited electrons are able to effectively tunnel through the Coulomb barrier in the case of a negatively charged grain. Note that, for  $Z < 0$ , we assume that the energy difference from the top of the valence band to the top of the potential well equals the work function; our expression for the electron affinity (eq. 4) does not give any information on the location of the valence band.

We estimate  $E_{\text{min}}(Z, a)$  as the energy for which the tunneling probability (evaluated using the WKB approximation) equals  $10^{-3}$ ; the tunneling probability rapidly increases as the excited electron energy increases above this value. The barrier consists of the Coulomb potential  $-(Z + 1)e^2/r$  and the image potential  $-e^2a^3/2r^2(r^2 - a^2)$ , where  $r$  is the distance from the center of the spherical grain.<sup>4</sup> We adopt the following expression for  $E_{\text{min}}$ , which reproduces the results of the WKB calculation fairly well when  $-(Z + 1)e^2/a \gtrsim 0.5 \text{ eV}$ :

$$E_{\text{min}}(Z < 0, a) = -(Z + 1) \frac{e^2}{a} \frac{a^{0.75}}{a^{0.75} + (27 \text{ \AA})^{0.75}} . \quad (7)$$

When  $-(Z + 1)e^2/a < 1 \text{ eV}$ , equation (7) overestimates  $E_{\text{min}}$  as defined above, with increasing severity as  $-(Z + 1)e^2/a \rightarrow 0$ . However, in this limit  $E_{\text{min}} \rightarrow 0$  as well, so that this overestimate will not substantially affect the photoemission calculations.

Thus, we adopt

$$h\nu_{\text{pet}} = W + \frac{14.4 \text{ eV}}{(a/\text{\AA})} \times \begin{cases} Z + \frac{1}{2} + (Z + 2) (0.6 \text{ \AA}/a) & , Z \geq 0 \\ -\frac{1}{2} + (Z + 1) (27 \text{ \AA})^{0.75} / [a^{0.75} + (27 \text{ \AA})^{0.75}] & , Z < 0 \end{cases} , \quad (8)$$

---

<sup>4</sup>Within a few  $\text{\AA}$  of the surface, the image potential deviates from the classical expression, and “saturates” to a constant value (see, e.g., Lang & Kohn 1971). However, this saturated portion of the potential does not enter into the WKB analysis.

with  $W = 4.4 \text{ eV}$  for carbonaceous grains and  $W = 8 \text{ eV}$  for silicates.

We adopt a very simple model for estimating the photoelectric yield  $Y(h\nu, Z, a)$ . We first consider the yield  $y'_0$  of electrons that traverse the surface layer, emerge from the grain surface, and have enough energy to overcome the image potential (we will call these “attempting” electrons). For  $Z < 0$ , every attempting electron will escape, but when  $Z \geq 0$ , some of these electrons have insufficient energy to escape to infinity and instead fall back to the grain. We assume the following form for  $y'_0$ :

$$y'_0 = y_0(\Theta)y_1(h\nu, a) \quad , \quad (9)$$

where the parameter  $\Theta$  is given by

$$\Theta = \begin{cases} h\nu - h\nu_{\text{pet}} + (Z + 1)e^2/a & , Z \geq 0 \\ h\nu - h\nu_{\text{pet}} & , Z < 0 \end{cases} \quad (10)$$

and the factor  $y_1(h\nu, a)$  accounts for the size-dependent geometrical yield enhancement discussed above;  $y_1$  depends on  $h\nu$  because the photon attenuation length  $l_a$  does.

We assume a parabolic energy distribution for the attempting electrons:<sup>5</sup>

$$f_E^0(E) = \frac{6(E - E_{\text{low}})(E_{\text{high}} - E)}{(E_{\text{high}} - E_{\text{low}})^3} \quad , \quad (11)$$

where  $f_E^0(E)dE$  gives the fraction of attempting electrons with energy (with respect to infinity) between  $E$  and  $E + dE$ . When  $Z < 0$ ,  $E_{\text{low}} = E_{\text{min}}$  (eq. 7) and  $E_{\text{high}} = E_{\text{min}} + h\nu - h\nu_{\text{pet}}$ ; when  $Z \geq 0$ ,  $E_{\text{low}} = -(Z + 1)e^2/a$  and  $E_{\text{high}} = h\nu - h\nu_{\text{pet}}$ .

Let  $y_2$  be the fraction of attempting electrons which escape to infinity:

$$y_2(h\nu, Z, a) = \begin{cases} \int_0^{E_{\text{high}}} dE f_E^0(E) = E_{\text{high}}^2(E_{\text{high}} - 3E_{\text{low}})/(E_{\text{high}} - E_{\text{low}})^3 & , Z \geq 0 \\ 1 & , Z < 0 \end{cases} \quad (12)$$

Our resulting expression for the photoelectric yield is

$$Y(h\nu, Z, a) = y_2(h\nu, Z, a) \min [y_0(\Theta)y_1(a, h\nu), 1] \quad . \quad (13)$$

Draine (1978) found that the following estimate for  $y_1$  reproduces Watson’s (1973) detailed results based on Mie theory, to within 20%:

$$y_1 = \left(\frac{\beta}{\alpha}\right)^2 \frac{\alpha^2 - 2\alpha + 2 - 2\exp(-\alpha)}{\beta^2 - 2\beta + 2 - 2\exp(-\beta)} \quad , \quad (14)$$

---

<sup>5</sup>A parabolic form is consistent with typical laboratory photoelectron distributions which drop to zero when  $E = 0$  and  $E = h\nu - W$  and peak somewhere in between (Draine 1978).

where  $\beta = a/l_a$  and  $\alpha = a/l_a + a/l_e$ .

Electron escape lengths for most materials reach a minimum in the vicinity of tens of eV and increase at higher and lower energies. The data are meager for electron energies below 10 eV, but Martin et al. (1987) found, for thin carbon films, that  $l_e$  fell into a broad minimum of 6 Å around 40 eV and rose to 9 Å at 6 eV. McFeely et al. (1990) found, for SiO<sub>2</sub>, that  $l_e$  varied from 5.7 to 6.8 Å for electron energies between 8 and 20 eV, and one might expect similar values for silicates. Bakes & Tielens (1994) assumed  $l_e = 10$  Å, independent of energy, and we use the same value here, for both graphite and silicates.

The photon attenuation length is given by

$$l_a = \frac{\lambda}{4\pi\text{Im}(m)} \quad , \quad (15)$$

where  $\lambda$  is the wavelength in vacuo and  $m(\lambda)$  is the complex refractive index. Graphite is a highly anisotropic material, so that the dielectric function is a tensor. This tensor may be diagonalized by choosing Cartesian coordinates with two of the axes lying in the “basal” plane; the third axis, normal to the basal plane, is called the “*c*-axis”. For graphite, we take

$$l_a^{-1} = \frac{4\pi}{\lambda} \left[ \frac{2}{3}\text{Im}(m_{\perp}) + \frac{1}{3}\text{Im}(m_{\parallel}) \right] \quad , \quad (16)$$

where  $m_{\perp}$  and  $m_{\parallel}$  are for the electric field perpendicular and parallel to the *c*-axis, respectively. In computing  $l_a$ , we use dielectric functions from Draine & Lee (1984)<sup>6</sup> and Laor & Draine (1993).

The final step in our yield prescription is to estimate  $y_0(\Theta)$  for graphite and silicates. For graphite, we follow Bakes & Tielens (1994) and choose  $y_0$  such that  $\pi a^2 Q_{\text{abs}} Y(h\nu, Z = 0, a = 4.2 \text{ \AA})$  approximately reproduces the photoionization cross section for coronene, as measured by Verstraete et al. (1990) ( $\pi a^2 Q_{\text{abs}}$  is the absorption cross section). This gives

$$y_0(\Theta) = \frac{7 \times 10^{-3} (\Theta/W)^5}{1 + 3.7 \times 10^{-2} (\Theta/W)^5} \quad , \quad (17)$$

---

<sup>6</sup> The “astronomical silicate” dielectric function  $\epsilon = \epsilon_1 + i\epsilon_2$  of Draine & Lee (1984), based on laboratory measurements of crystalline olivine in the ultraviolet (Huffman & Stapp 1973), contains a feature at  $6.5\mu\text{m}^{-1}$ . Kim & Martin (1995) have pointed out that this feature, which is of crystalline origin, is not present in the observed interstellar extinction or polarization. We have therefore excised this feature from  $\epsilon_2$ , and recomputed  $\epsilon_1$  using the Kramers-Kronig relation (Draine & Lee 1984). The resulting “smoothed astronomical silicate” dielectric functions are available on the World Wide Web at <http://www.astro.princeton.edu/~draine/index.html>

with  $W = 4.4 \text{ eV}$ . Draine (1978) shows, in his Figure 1, that the bulk graphite yield measured by Feuerbacher & Fitton (1972) is unusually low, and lies more than an order of magnitude below the yields for anthracene (Fujihira, Hirooka, & Inokuchi 1973). It is important to note that our equation (17) gives yields that substantially exceed those measured for bulk graphite.<sup>7</sup> This apparent inconsistency could imply one or more of the following: 1. The yield for bulk graphite differs substantially from that for bulk coronene. 2. The measured yields for bulk graphite are wrong. 3. Our prescription for  $y_1(a, h\nu)$  is wrong. Clearly, the adopted yields for graphite grains are highly uncertain.

The situation for silicates is no better. Feuerbacher et al. (1972) measured the yield for a powdered sample of lunar dust, and found that  $Y$  decreases rapidly as photon energy is decreased below  $14 \text{ eV}$ . However, they noted that the use of the powdered sample might result in yields that are too low. Thus, we choose  $y_0$  for silicates such that the bulk yield somewhat exceeds the results of Feuerbacher et al. at  $14 \text{ eV}$ , but does not drop as rapidly for lower values of  $h\nu$ :

$$y_0(\Theta) = \frac{0.5 (\Theta/W)}{1 + 5 (\Theta/W)} \quad , \quad (18)$$

with  $W = 8 \text{ eV}$ .

In Figure 4 we plot  $Y(h\nu)$  for neutral graphite and silicate grains of several sizes.

### 2.3.2. Photoelectric Ejection of Attached Electrons (Photodetachment)

When  $Z < 0$ , the  $-Z$  attached electrons occupy energy levels above the valence band, if the latter is full in the neutral. We take the photodetachment threshold energy  $h\nu_{\text{pdt}}$  to be

$$h\nu_{\text{pdt}}(Z < 0) = EA(Z + 1, a) + E_{\text{min}}(Z, a) \quad (19)$$

with electron affinities  $EA$  given by equations (4) and (5), and  $E_{\text{min}}$  by (7). Bakes & Tielens (1994) neglected  $E_{\text{min}}(Z, a)$  and took  $h\nu_{\text{pdt}} = EA(Z + 1, a)$ . We assume that  $E = h\nu - h\nu_{\text{pdt}}$  for photodetached electrons, since attached electrons lie in a narrow range of energies.

We assume that an oscillator strength  $f_{\text{pdt}}$  is associated with photodetachment transitions to the continuum. The photodetachment cross section  $\sigma_{\text{pdt}}(h\nu)$  has been

---

<sup>7</sup>For example, at  $h\nu = 10 \text{ eV}$ , where Feuerbacher & Fitton (1972) measured a yield of  $8 \times 10^{-3}$  for bulk graphite, our equation (17) gives  $y_0 = 2.1 \times 10^{-2}$ , a factor 2.6 larger than the laboratory value. For comparison, the Bakes & Tielens (1994) expression gives  $y_0 = 7.8 \times 10^{-2}$ , an order of magnitude larger than the experimental value.

measured for  $\text{C}_6\text{F}_6^-$  (Christophorou, Datskos, & Faidas 1994). The measured cross section has considerable structure, but can be roughly approximated by

$$\sigma_{\text{pdt}}(Z, a) = -Z \frac{2\pi e^2 h f_{\text{pdt}}}{3m_e c \Delta E} \frac{x}{(1 + x^2/3)^2} \quad , \quad (20)$$

where  $x \equiv (h\nu - h\nu_{\text{pdt}})/\Delta E$  and the peak in  $\sigma_{\text{pdt}}$  occurs at  $h\nu = h\nu_{\text{pdt}} + \Delta E$ . We take  $\Delta E = 3 \text{ eV}$  and  $f_{\text{pdt}} = 0.5$ ; thus

$$\sigma_{\text{pdt}}(h\nu, Z, a) = 1.2 \times 10^{-17} \text{ cm}^2 |Z| \frac{x}{(1 + x^2/3)^2} \quad \text{for } Z < 0. \quad (21)$$

## 2.4. Grain Charging

Since the photoemission depends on the grain charge, it is necessary to know the distribution of charge states for the grains. In statistical equilibrium,

$$f_Z(Z)[J_{\text{pe}}(Z) + J_{\text{ion}}(Z)] = f_Z(Z+1)J_e(Z+1) \quad , \quad (22)$$

where  $f_Z(Z)$  is the probability for the grain charge to be  $Ze$ ,  $J_{\text{pe}}$  is the photoemission rate,  $J_{\text{ion}}$  is the positive ion accretion rate, and  $J_e$  is the electron accretion rate.

Bakes & Tielens (1994) discuss the most positive and most negative charges that a grain could possibly acquire ( $Z_{IP}e$  and  $Z_{EA}e$ , respectively). The most positive charge is one proton charge more than the highest charge for which an electron can be ejected, i.e. for which  $h\nu_{\text{pet}} = IP < h\nu_{\text{max}}$ , the maximum photon energy in the radiation field ( $= 13.6 \text{ eV}$ , in an H I region). Thus,

$$Z_{IP} = \text{int} \left[ \left( \frac{h\nu_{\text{max}} - W}{14.4 \text{ eV}} \frac{a}{\text{\AA}} + \frac{1}{2} - \frac{0.6 \text{ \AA}}{a} \right) \left( 1 + \frac{0.6 \text{ \AA}}{a} \right)^{-1} \right] \quad , \quad (23)$$

where  $\text{int}[x]$  denotes the greatest integer less than  $x$ . The negative threshold charge  $Z_{EA}e$  is the most negative charge for which autoionization does not occur. Bakes & Tielens (1994) assume that this requires  $EA(Z_{EA} + 1) > 0$ . However, large grains can be charged more negatively without emitting a substantial electron current when the tunneling probability is low. We take the autoionization threshold potential  $U_{\text{ait}}$  to be that at which the electron current is  $\approx 10^{-6} \text{ s}^{-1}$ ; we evaluate the tunneling probability using the WKB approximation and assume an oscillation frequency of  $\approx 2 \times 10^8 \text{ s}^{-1} (\text{cm}/a)$ . We find

$$\frac{-U_{\text{ait}}}{V} \approx \begin{cases} 3.9 + 0.12 \left( \frac{a}{\text{\AA}} \right) & , \text{ for graphite} \\ 2.5 + 0.07 \left( \frac{a}{\text{\AA}} \right) + 8 \left( \frac{\text{\AA}}{a} \right) & , \text{ for silicate} \end{cases} \quad ; \quad (24)$$

this agrees very well with Draine & Salpeter’s (1979) simple estimate of the potential at which field emission becomes important. The negative threshold charge is given by

$$Z_{EA} = \text{int} \left[ \frac{U_{\text{ait}}}{14.4 \text{ eV}} \frac{a}{\text{\AA}} \right] + 1 \quad . \quad (25)$$

By iteratively applying equation (22) and normalizing,  $f_Z$  can be found for all  $Z$ .

The photoemission rate is given by

$$J_{\text{pe}} = \pi a^2 \int_{\nu_{\text{pet}}}^{\nu_{\text{max}}} d\nu Y Q_{\text{abs}}(\nu) \frac{cu_\nu}{h\nu} + \int_{\nu_{\text{pdt}}}^{\nu_{\text{max}}} d\nu \sigma_{\text{pdt}}(\nu) \frac{cu_\nu}{h\nu} \quad , \quad (26)$$

where  $Q_{\text{abs}}$  is the absorption efficiency,  $u_\nu$  is the radiation energy density per frequency interval, and  $c$  is the speed of light. The second term in equation (26) is only present when  $Z < 0$ . Bakes & Tielens (1994) assumed  $Q_{\text{abs}} \propto a$ , valid for grains with  $a \lesssim 100 \text{ \AA}$ . Since we consider larger grains, we evaluate  $Q_{\text{abs}}$  using a Mie theory code derived from BHMIE (Bohren & Huffman 1983), with dielectric functions as described by Draine & Lee (1984)<sup>8</sup> and Laor & Draine (1993). For graphite grains, we adopt the usual “1/3 – 2/3” approximation, and assume that  $Q_{\text{abs}} = [Q_{\text{abs}}(\epsilon_{\parallel}) + 2Q_{\text{abs}}(\epsilon_{\perp})]/3$ , where  $\epsilon_{\parallel}$  and  $\epsilon_{\perp}$  are the components of the graphite dielectric tensor for the electric field parallel and perpendicular to the  $c$ -axis, respectively. Draine & Malhotra (1993) showed that the 1/3 – 2/3 approximation is sufficiently accurate for extinction curve modelling.

The accretion rates are given by

$$J_i(Z) = n_i s_i(Z) \left( \frac{8kT}{\pi m_i} \right)^{1/2} \pi a^2 \tilde{J}(\tau_i, \xi_i) \quad , \quad (27)$$

where  $n_i$  is the number density of species  $i$ , the sticking coefficient  $s_i(Z)$  is the probability that species  $i$  will transfer its charge if it reaches the surface of a grain of charge  $Ze$ ,  $m_i$  is the particle mass,  $T$  is the gas temperature, and  $\tilde{J}$  is a function of  $\tau_i \equiv akT/q_i^2$  and  $\xi_i \equiv Ze/q_i$  ( $q_i$  is the charge of species  $i$  and  $k$  is the Boltzmann constant). Expressions for  $\tilde{J}$  can be found in Draine & Sutin (1987). The electron and ion sticking coefficients  $s_e$  and  $s_i$  are discussed below in §3.

### 3. Sticking Coefficients

---

<sup>8</sup>See footnote 6.

### 3.1. Electrons

A low-energy electron impinging on a macroscopic solid surface has some probability  $p_{es}$  of elastic scattering. We will assume that  $p_{es} \approx 0.5$ , so that the maximum possible value of the sticking coefficient  $s_e$  would be  $(1 - p_{es}) \approx 0.5$ .

#### 3.1.1. Attachment to Neutral Grains

We first consider electron attachment to neutral grains. If the electron affinity is positive (as it is when  $a > 3.5 \text{ \AA}$ , which we take in §6 to be the lower cutoff for the grain size distribution), then the approaching electron accelerates due to its polarization of the grain, arriving at the surface with a kinetic energy of order  $EA$ . Even if it enters the grain material [with probability  $(1 - p_{es})$ ], the electron may fail to undergo an inelastic scattering event, in which case it passes through the grain and returns to infinity. The probability of undergoing inelastic scattering is approximately  $(1 - e^{-a/l_e})$ , where  $l_e \approx 10 \text{ \AA}$ , the “electron escape length” (discussed above), is roughly the mean free path against inelastic scattering within the grain material.

If the impinging electron does undergo inelastic scattering, then it transfers some of its energy to internal degrees of freedom of the grain; if the energy so transferred exceeds the initial kinetic energy ( $\sim 1.5kT$ ), then the electron is trapped by the grain potential. However, until the grain radiates this energy away, there is a nonzero probability per unit time that the internal degrees of freedom of the grain will transfer enough energy back to the electron to eject it. Let  $p_{\text{rad}}$  be the probability of “radiative stabilization” of the negatively charged grain, i.e. the probability of radiating away  $\sim kT$  of energy before the electron is ejected. We expect  $p_{\text{rad}} \rightarrow 1$  for macroscopic grains, but  $p_{\text{rad}} < 1$  for grains with a small number of internal degrees of freedom. The electron attachment sticking coefficient can then be written as the product of three factors:

$$s_e(Z = 0) \approx (1 - p_{es}) (1 - e^{-a/l_e}) p_{\text{rad}} . \quad (28)$$

The stabilization probability  $p_{\text{rad}}$  can be estimated from the electron affinity  $EA$ , the density of states of the excited negatively charged grain created by the electron attachment, and the probability per time of photon emission from the excited grain (Allamandola, Tielens, & Barker 1989; Tielens 1993). However, since these parameters are poorly known, we will instead adopt an empirical approach.

In Figure 6 we show sticking coefficients  $s_e = \langle \sigma v \rangle / [(8kT/\pi m_e)^{1/2} \pi a^2 \tilde{J}]$  for various hydrocarbon molecules, where  $\tilde{J}(akT/e^2, 0)$  is given by Draine & Sutin (1987) and the rate

coefficients  $\langle\sigma v\rangle$  for electron attachment are determined experimentally. Also shown in Figure 6 is a semiempirical fit:

$$s_e(Z = 0) = 0.5 \left(1 - e^{-a/l_e}\right) \frac{1}{1 + e^{(20-N_C)}} \quad , \quad (29)$$

where  $N_C$  is the number of atoms other than H in the molecule, and  $l_e = 10^{-7}$  cm.

The measured sticking coefficients for  $N_C \leq 20$  are in reasonable agreement with our semiempirical fit (eq. 29). It is notable that Tobita et al. (1992) found that in many cases the sticking coefficient *increases* when the electron energy increases. For example, the sticking coefficients for tetracene  $C_{18}H_{12}$  and perylene  $C_{20}H_{12}$  would be larger by an order of magnitude for gas temperature  $T \approx 2000$ K, bringing them up to or even above the values given by equation (29).

The measured  $s_e$  for  $C_{60}$  and  $C_{70}$  at  $T \leq 500$ K are remarkably low, probably due to the unusual rigidity and symmetry of these molecules. For  $C_{60}$ , the symmetry forbids capture of  $s$ -wave electrons, and the centrifugal barrier to  $p$ -wave electrons results in an apparent activation energy of 0.26eV (Tossati & Manini 1994). At high temperatures the sticking coefficients for  $C_{60}$  and  $C_{70}$  are close to the values given by equation (29).

We adopt equation (29) for  $s_e(Z = 0)$  for silicates as well as for carbonaceous grains, since no laboratory data are available for silicates. In this case,  $N_C$  is just a parameter defined by equation (1).

### 3.1.2. Attachment to Negatively Charged Grains

We take the electron sticking coefficient for negatively charged grains to be

$$s_e(Z < 0) = s_e(Z = 0) \min \{1, \exp [EA(Z)/kT]\} \quad , \quad (30)$$

since, if  $EA(Z) < 0$ , an electron must have a kinetic energy of at least  $|EA(Z)|$  in order to stick to the grain.

### 3.1.3. Recombination with Positively Charged Grains

Electrons arriving at positively charged grains are expected to recombine provided that (1) they do not reflect elastically from the surface and (2) they are able to scatter inelastically before traversing the grain. For small molecules the energy released generally results in dissociation, but for hydrocarbons this most likely results in only the loss of an

H atom, with the carbon skeleton remaining intact. The sticking coefficient is therefore expected to be

$$s_e(Z > 0) \approx (1 - p_{es}) [1 - \exp(-a/l_e)] \approx 0.5 [1 - \exp(-a/l_e)] \quad . \quad (31)$$

Figure 7 shows measured  $s_e$  for electron recombination with positive hydrocarbon ions, together with fitting function (31). The measured sticking coefficients generally agree with equation (31) to within a factor of 2 except for the values measured for naphthalene  $C_{10}H_8^+$  and phenanthrene  $C_{14}H_{10}^+$ , which are smaller than predicted by factors of 5 and 3, respectively. Why they should be smaller is unclear.

### 3.2. Ions

Ions of interest ( $H^+$  and  $C^+$ ) have large ionization potentials, so we assume that they have a high probability of seizing an electron if they arrive at the surface of a grain, whether charged or neutral. While this assumption would be invalid for grains which are already highly positively charged, in practice the rate of arrival of positive ions at the surface of such a grain is in any case negligible. We compute the contribution of ions to the charging rate using equation (27) with  $s_i = 1$ .

## 4. Ambient Conditions

### 4.1. Radiation Fields

For most calculations, we adopt a blackbody spectrum for the radiation field, with color temperature  $T_c$  and dilution factor  $w$ , so that  $u_\nu = 4\pi w B_\nu(T_c)/c$ . It is convenient to characterize the radiation intensity by  $G \equiv u_{\text{rad}}^{\text{uv}}/u_{\text{Hab}}^{\text{uv}}$ , where  $u_{\text{rad}}^{\text{uv}}$  is the energy density in the radiation field between 6 eV and 13.6 eV and  $u_{\text{Hab}}^{\text{uv}} = 5.33 \times 10^{-14} \text{ erg cm}^{-3}$  is the Habing (1968) estimate of the starlight energy density in this range.<sup>9</sup> The radiation is cut off at 13.6 eV.

For the diffuse ISM, we adopt the average interstellar radiation field (ISRF) spectrum in the solar neighborhood, as estimated by Mezger, Mathis, & Panagia (1982) and Mathis,

---

<sup>9</sup> For comparison, the interstellar radiation field estimated by Draine (1978) has  $u = 8.93 \times 10^{-14} \text{ erg cm}^{-3}$  between 6 and 13.6 eV, or  $G = 1.68$ .

Mezger, & Panagia (1983):

$$\nu u_\nu^{\text{ISRF}} = \begin{cases} 0 & , h\nu > 13.6 \text{ eV} \\ 3.328 \times 10^{-9} \text{ erg cm}^{-3} (h\nu / \text{eV})^{-4.4172} & , 11.2 \text{ eV} < h\nu < 13.6 \text{ eV} \\ 8.463 \times 10^{-13} \text{ erg cm}^{-3} (h\nu / \text{eV})^{-1} & , 9.26 \text{ eV} < h\nu < 11.2 \text{ eV} \\ 2.055 \times 10^{-14} \text{ erg cm}^{-3} (h\nu / \text{eV})^{0.6678} & , 5.04 \text{ eV} < h\nu < 9.26 \text{ eV} \\ (4\pi\nu/c) \sum_{i=1}^3 w_i B_\nu(T_i) & , h\nu < 5.04 \text{ eV} \end{cases} ; \quad (32)$$

the dilution factors and blackbody temperatures are given in Table 1. The total energy density in the ISRF of equation (32) is  $u = 8.64 \times 10^{-13} \text{ erg cm}^{-3}$ , with  $u_{\text{rad}}^{\text{uv}} = 6.07 \times 10^{-14} \text{ erg cm}^{-3}$  in the 6-13.6 eV interval, or  $G = 1.13$ .

The spectrum-averaged absorption efficiency factor is

$$\langle Q_{\text{abs}} \rangle \equiv \frac{\int_0^{\nu_H} Q_{\text{abs}} u_\nu d\nu}{\int_0^{\nu_H} u_\nu d\nu} , \quad (33)$$

where  $Q_{\text{abs}}\pi a^2$  is the absorption cross section. In Figure 5 we display  $\langle Q_{\text{abs}} \rangle$  for the ISRF and blackbody spectra with various values of  $T_c$ .

## 4.2. Scaling Law

The photoelectric emission is dependent on the ambient conditions, which can be characterized by the shape of the radiation spectrum, the gas temperature  $T$ , and one additional parameter, depending on the ratio  $G/n_e$ , which we take to be  $G\sqrt{T}/n_e$ .

Unless otherwise noted, we will display results for a blackbody spectrum with  $T_c = 3 \times 10^4 \text{ K}$ , cut off at 13.6 eV. In Figure 8, charge distributions are plotted for graphite grains with various sizes in various environments. In Figure 9, the average electrostatic potential,  $\langle U \rangle$ , is plotted as a function of grain size for two values of  $T$ , 100 K and 1000 K, and five values of  $G\sqrt{T}/n_e$ , ranging from  $10^2$  to  $10^6 \text{ K}^{1/2} \text{ cm}^3$ . We also provide results for conditions appropriate for the cold neutral medium (ISRF,  $T = 100 \text{ K}$ ,  $n_e = 0.03 \text{ cm}^{-3}$ ,  $G\sqrt{T}/n_e = 330$ ) and the warm neutral medium (ISRF,  $T = 6000 \text{ K}$ ,  $n_e = 0.03 \text{ cm}^{-3}$ ,  $G\sqrt{T}/n_e = 2600$ ). Note that for given  $G\sqrt{T}/n_e$ , the computed potentials show hardly any dependence on  $T$ .

For low values of  $G\sqrt{T}/n_e$ , the grains can be negatively charged. This is especially so for grains with  $a \lesssim l_e \approx 10 \text{ \AA}$ , for which the photoemission rate scales approximately with  $a^3$  rather than  $a^2$ . However, once  $a \lesssim 4 \text{ \AA}$ , the potential rapidly rises to positive values; this is a consequence of the rapid decrease in  $s_e$  for grains with  $Z \leq 0$  as  $a$  decreases in this range (eq. 29). The wiggles in the curves for high  $G\sqrt{T}/n_e$  are due to saturation at the positive

threshold charge  $Z_{IP}$ . As the grain size increases,  $f_Z(Z_{IP}) \rightarrow 1$ , until the size at which  $Z_{IP}$  increases by 1 is reached. Thus, although  $\langle Z \rangle$  increases monotonically with  $a$ , it plateaus until  $Z_{IP}$  is incremented, so that  $\langle U \rangle$  decreases. Once  $Z_{IP}$  does increment,  $\langle U \rangle$  does not abruptly increase, because the photoemission rate depends on  $h\nu - h\nu_{\text{pet}}$  and  $h\nu - h\nu_{\text{pdt}}$ ; thus charge is gradually concentrated in the next higher charge state as  $a$  increases.

To see why  $G\sqrt{T}/n_e$  is a good parameter to describe grain charging, we make the approximation that the charge state on any grain remains constant, i.e.

$$J_e = J_{\text{pe}} + J_{\text{ion}} \quad . \quad (34)$$

We neglect  $J_{\text{ion}}$  by virtue of the large proton mass and consider a positively charged grain with  $U \sim 1$  V. The Draine & Sutin (1987) expression for  $\tilde{J}$  for a grain with static dielectric constant  $\epsilon(0) \gg 1$  and  $\xi_i < 0$  is

$$\tilde{J} \approx \left(1 - \frac{\xi_i}{\tau_i}\right) \left[1 + \left(\frac{2}{\tau_i - 2\xi_i}\right)^{1/2}\right] \quad , \quad (35)$$

which expands, for  $eU/kT \gg 1$ , to give

$$\tilde{J} \approx \frac{eU}{kT} \left(1 + Z^{-1/2}\right) \quad . \quad (36)$$

We express

$$J_{\text{pe}} \propto G \langle Q_{\text{abs}} \rangle a^2 g(U, a) \quad , \quad (37)$$

where  $\langle Q_{\text{abs}} \rangle$  is the average value of  $Q_{\text{abs}}$  over the range of absorbed photon energies. Here  $g(U, a)$  must be a decreasing function of  $U$  and  $g$  depends on  $a$  through the size dependence of the yield  $Y$  (see equations 13 and 14). Thus,

$$\frac{U \left(1 + Z^{-1/2}\right)}{g(U, a)} \propto \langle Q_{\text{abs}} \rangle \frac{G\sqrt{T}}{n_e} \quad . \quad (38)$$

Note that this result applies only when  $G/n_e$  is large enough (for given  $T$  and  $a$ ) to keep the grains strongly positively charged (with  $eU \gtrsim kT$ ). For low values of  $G/n_e$ ,  $J_{\text{ion}}$  plays a significant role in the grain charging. This introduces an additional dependence on the ionization fraction  $x \equiv n_e/n_{\text{H}}$ , since for the lowest  $x$  (i.e.  $x \lesssim 2 \times 10^{-4}$ ), the ions are predominantly  $\text{C}^+$ , whereas  $\text{H}^+$  dominates for higher  $x$ , and  $J_{\text{ion}}$  depends on the ion mass. We assume  $\text{H}^+$  in our calculations for the CNM and WNM and  $\text{C}^+$  in our other calculations. For the values of  $G\sqrt{T}/n_e$  and  $T$  considered here, the dependence on ion mix is only significant for the smallest grains, and even then extreme changes in the ion mix lead to only modest changes in the results. In Figure 10 we display  $(G\sqrt{T}/n_e)_0$ , the value

of the charging parameter for which  $\langle Z \rangle = 0$ , for graphite and silicate grains, a blackbody radiation field with  $T_c = 3 \times 10^4$  K, and various gas temperatures. As  $a$  decreases beyond  $\approx 4$  Å it becomes very difficult for the grains to charge negatively, because  $s_e$  becomes very small for  $Z \leq 0$ ; thus the curves plunge sharply there.

Incidentally, the presence of  $\langle Q_{\text{abs}} \rangle$  in equation (38) explains the maxima in  $\langle U \rangle$  at  $a \sim 100$  Å (see Figure 9), since  $Q_{\text{abs}}$  peaks for  $2\pi a \sim \lambda$ , and the photoelectric emission is primarily from radiation with  $\lambda \sim 1000$  Å.

## 5. Photoelectric Heating Efficiencies

The gas heating rate per grain due to photoelectric emission is given by

$$\Gamma'_{\text{pe}}(a) = \sum_Z f_Z(Z) \left[ \Gamma'_{\text{pe,v}}(a) + \Gamma'_{\text{pd}}(a) \right] \quad . \quad (39)$$

The contribution from the photoemission of valence electrons is

$$\Gamma'_{\text{pe,v}}(a) = \pi a^2 \int_{\nu_{\text{pet}}}^{\nu_{\text{max}}} d\nu Y Q_{\text{abs}} \frac{c u_\nu}{h\nu} \int_{E_{\text{min}}}^{E_{\text{max}}} dE f_E(E) E \quad , \quad (40)$$

where  $E_{\text{min}} = 0$  when  $Z \geq 0$  and is given by equation (7) when  $Z < 0$ , and  $E_{\text{max}} = h\nu - h\nu_{\text{pet}} + E_{\text{min}}$ . The photoelectron energy distribution  $f_E(E) = f_E^0(E)/y_2$  (see eq. 11 and the discussion following it). When  $Z < 0$ , the contribution from photodetachment is given by

$$\Gamma'_{\text{pd}}(a) = \int_{\nu_{\text{pdt}}}^{\nu_{\text{max}}} d\nu \sigma_{\text{pdt}}(\nu) \frac{c u_\nu}{h\nu} (h\nu - h\nu_{\text{pdt}} + E_{\text{min}}) \quad . \quad (41)$$

We compute the total efficiency for conversion of absorbed radiation into gas heating,

$$\epsilon_\Gamma(a) = \frac{\Gamma'_{\text{pe}}(a) - \Lambda'(a)}{\pi a^2 c u_{\text{rad}} \langle Q_{\text{abs}} \rangle} \quad . \quad (42)$$

Here  $\Lambda'(a)$  is the rate of energy removal from the gas due to the accretion of charged particles onto the grain, and is given by

$$\Lambda'(a) = \sum_i n_i s_i \left( \frac{8kT}{\pi m_i} \right)^{1/2} \pi a^2 \tilde{\Lambda}(\tau_i, \xi_i) kT \quad , \quad (43)$$

where the sum runs over electrons and ions and  $\tau_i$  and  $\xi_i$  are defined below equation (27). Expressions for  $\tilde{\Lambda}$  can be found in Draine & Sutin (1987).

Figures 11 through 13 show results for the gas heating efficiency for the same conditions for which potentials were displayed in Figure 9. The heating efficiency generally decreases

as grain size  $a$  increases. For low values of  $G\sqrt{T}/n_e$ , this results primarily from the size-dependent yield factor  $y_1$  (equation 14); the heating efficiency levels off at  $a \sim 10^3 \text{ \AA}$ , where  $y_1$  levels off. For higher  $G\sqrt{T}/n_e$ , high grain potentials quench the photoemission and result in much lower heating efficiencies; in these cases the smallest grains (with  $a \lesssim 100 \text{ \AA}$ ), with somewhat lower potentials (see Figure 9), dominate the photoelectric heating. The heating efficiencies drop dramatically when  $a \lesssim 4 \text{ \AA}$ , as  $s_e(Z \leq 0)$  decreases rapidly and the grains charge positively.

## 6. Grain Size Distributions

The classic MRN grain size distribution was derived to reproduce the observed extinction through the diffuse ISM using bare graphite and silicate grains (Mathis, Rumpl, & Nordsieck 1977); the expression for the grain number density in this model is

$$dn_{\text{gr}} = C n_{\text{H}} a^{-3.5} da, \quad a_{\text{min}} < a < a_{\text{max}} \quad (44)$$

with  $C = 10^{-25.13}$  ( $10^{-25.11}$ )  $\text{cm}^{3.5}$  for graphite (silicate) grains (Draine & Lee 1984),  $a_{\text{min}} = 50 \text{ \AA}$ , and  $a_{\text{max}} = 0.25 \mu\text{m}$ .

Since the development of the MRN model, more observational constraints have become available. Observations of 3 to  $60 \mu\text{m}$  infrared emission, presumably generated by grains small enough to reach temperatures of 30 to 300 K or more upon the absorption of a single starlight photon (see e.g. Draine & Anderson 1985), imply a population of very small grains (with  $a < 50 \text{ \AA}$ ). The non-detection of the  $10 \mu\text{m}$  silicate feature in emission from diffuse clouds (Mattila et al. 1996; Onaka et al. 1996) appears to rule out silicate grains as a major component of the  $a \lesssim 15 \text{ \AA}$  population. Emission features at 3.3, 6.2, 7.7, 8.6, and  $11.3 \mu\text{m}$  (see Sellgren 1994 for a review) have been identified as C-H and C-C stretching and bending modes in polycyclic aromatic hydrocarbons (Léger & Puget 1984), suggesting that the graphite population extends down into the molecular regime. Graphite grains with volume  $\lesssim 4\pi(3.5 \text{ \AA})^3/3$  are expected to be unstable against sublimation in the interstellar radiation field (Guhathakurta & Draine 1989). Recent observations of dust-correlated microwave emission has been attributed to the very small grain population (Draine & Lazarian 1998a).

The abundance of very small grains required to generate the observed IR emission from the diffuse ISM is not yet well-known. In the model of Désert, Boulanger, & Puget (1990), 9% of the cosmic C is in polycyclic aromatic hydrocarbon (PAH) molecules with less than 540 C atoms (equal to the number of C atoms in a spherical graphite grain with  $a \approx 10 \text{ \AA}$ ). Draine & Lazarian (1998b) estimated the electric dipole radiation from spinning grains. They considered an MRN distribution with  $a_{\text{min}}$  extended down to  $3.5 \text{ \AA}$  for graphite plus an

additional population of very small carbonaceous grains with a log-normal size distribution:

$$\frac{1}{n_{\text{H}}} \frac{dn_{\text{gr}}}{da} = D(a) \equiv \frac{B}{a} \exp \left\{ -\frac{1}{2} \left[ \frac{\ln(a/a_0)}{\sigma} \right]^2 \right\} , \quad a > 3.5 \text{ \AA} \quad (45)$$

$$B = \frac{3}{(2\pi)^{3/2}} \frac{\exp(-4.5\sigma^2)}{a_0^3 \rho \sigma} \frac{4.0 \times 10^{-4} m_{\text{C}} f_{\text{g}}}{\left\{ 1 + \text{erf}[3\sigma/\sqrt{2} + \ln(a_0/3.5 \text{ \AA})/\sigma\sqrt{2}] \right\}} , \quad (46)$$

where  $f_{\text{g}}$  is the fraction of the cosmic C in the log-normal population,  $m_{\text{C}}$  is the mass of a C atom, and  $\rho = 1.5 \text{ g cm}^{-3}$  is the carbon density in the small grains. Draine & Lazarian adopted  $a_0 = 3 \text{ \AA}$  and  $\sigma = 0.5$  and found that the dipole radiation could account for the dust-correlated component of the diffuse Galactic microwave emission if  $f_{\text{g}} \approx 0.05$ .

Our goal here is to find an overall grain size distribution which includes very small carbonaceous grains and is consistent with the observed extinction. For simplicity, we assume that the grains consist of bare graphite and silicate spheres, with dielectric functions as given by Draine & Lee (1984) and Laor & Draine (1993). (We use the “smoothed astronomical silicate” dielectric functions, as discussed in footnote 6.) We adopt the following form for the distribution:

$$\frac{1}{n_{\text{H}}} \frac{dn_{\text{gr}}}{da} = D(a) + \frac{C_{\text{g}}}{a} \times \begin{cases} (a/a_{\text{t,g}})^{\alpha_{\text{g}}} , & 3.5 \text{ \AA} < a < a_{\text{t,g}} \\ (a/a_{\text{t,g}})^{\beta_{\text{g}}} \exp [(a_{\text{t,g}}/a_{\text{c,g}})^3 - (a/a_{\text{c,g}})^3] , & a > a_{\text{t,g}} \end{cases} \quad (47)$$

for graphite and

$$\frac{1}{n_{\text{H}}} \frac{dn_{\text{gr}}}{da} = \frac{C_{\text{s}}}{a} \times \begin{cases} (a/a_{\text{t,s}})^{\alpha_{\text{s}}} , & a_{\text{min,s}} < a < a_{\text{t,s}} \\ (a/a_{\text{t,s}})^{\beta_{\text{s}}} \exp [(a_{\text{t,s}}/a_{\text{c,s}})^3 - (a/a_{\text{c,s}})^3] , & a > a_{\text{t,s}} \end{cases} \quad (48)$$

for silicate. We adopt the same values for  $a_0$  and  $\sigma$  as Draine & Lazarian (1998b).<sup>10</sup> For a given value of  $f_{\text{g}}$ , we seek the best fit to the extinction by varying the powers  $\alpha_{\text{g}}$ ,  $\beta_{\text{g}}$ ,  $\alpha_{\text{s}}$ , and  $\beta_{\text{s}}$ ; the transition sizes  $a_{\text{t,g}}$  and  $a_{\text{t,s}}$ ; the lower cutoff size  $a_{\text{min,s}}$ ; the upper cutoff parameters  $a_{\text{c,g}}$  and  $a_{\text{c,s}}$ ; and the total volume per H in both the graphite and silicate distributions.

The extinction at wavelength  $\lambda$  is given by

$$A(\lambda) = (2.5\pi \log e) \int d \ln a \frac{dN_{\text{gr}}(a)}{da} a^3 Q_{\text{ext}}(a, \lambda) , \quad (49)$$

where  $N_{\text{gr}}(a)$  is the column density of grains with size  $\leq a$  and  $Q_{\text{ext}}$  is the extinction efficiency factor, evaluated using Mie theory. The extinction curve (i.e. the functional

---

<sup>10</sup>Since the grains in the log-normal population all have  $a \ll \lambda$ , the values of  $a_0$  and  $\sigma$  do not affect the extinction; all that matters is the value of  $f_{\text{g}}$ .

dependence of the extinction on the wavelength) varies depending upon the interstellar environment through which the starlight passes. Cardelli, Clayton, & Mathis (1989, CCM) found that this dependence can be characterized fairly well by a single parameter, which they took to be  $R_V \equiv A(V)/E(B - V)$ , the ratio of visual extinction to reddening. CCM have fitted the average extinction curve  $A(\lambda)/A(V)$  as functions of  $\lambda$  and  $R_V$ . For the diffuse ISM,  $R_V \approx 3.1$ ; higher values are observed for dense clouds. Bohlin, Savage, & Drake (1978) found that the ratio of the total neutral hydrogen column density  $N_H$  (including both atomic and molecular forms) to  $E(B - V)$  is fairly constant for the diffuse ISM, with value  $5.8 \times 10^{21} \text{ cm}^{-2}$ . This provides the normalization for the extinction curve:  $A(V)/N_H = 5.3 \times 10^{-22} \text{ cm}^2$ . The normalization is less clear for dense clouds, because of the difficulty in measuring  $N_H$ . CCM found that  $A(\lambda)/A(I)$  appears to be independent of  $R_V$  for  $\lambda > 0.9 \mu\text{m}$  (= I band) suggesting that the diffuse cloud value of  $A(I)/N_H = 2.6 \times 10^{-22} \text{ cm}^2$  may also hold for dense clouds (see, e.g., Draine 1989); we adopt this normalization.

We use the Levenberg-Marquardt method, as implemented in Press et al. (1992), to fit the continuous extinction between  $0.3 \mu\text{m}^{-1}$  and  $10 \mu\text{m}^{-1}$ , and demand that  $a_{\text{min}}^s \geq 15 \text{ \AA}$ . We evaluate the extinction at 100 points, equally spaced in  $\ln \lambda^{-1}$ , and minimize the error function  $\chi_1^2 = \sum_i (\ln A_{\text{obs}} - \ln A_{\text{mod}})^2 / \sigma_i^2$ , where  $A_{\text{obs}}$  is the average “observed” extinction as given by CCM for a given value of  $R_V$ ,  $A_{\text{mod}}$  is the extinction computed for the model (equation 49), and the  $\sigma_i$  are weights. When evaluating  $A_{\text{mod}}$ , we verify that the integral in equation (49) is evaluated accurately.

For  $A_{\text{obs}}$ , we adopt the CCM parametrization for  $3.3 \mu\text{m}^{-1} < \lambda^{-1} < 10 \mu\text{m}^{-1}$ . For  $1.1 \mu\text{m}^{-1} < \lambda^{-1} < 3.3 \mu\text{m}^{-1}$ , we employ the extinction properties from O’Donnell (1994), slightly modified to join smoothly with CCM at  $1.1 \mu\text{m}^{-1}$  and  $3.3 \mu\text{m}^{-1}$ . The CCM expression for  $\lambda^{-1} < 1.1 \mu\text{m}^{-1}$  was derived by fitting the data of Rieke & Lebofsky (1985) with a power law; the resulting power law index is 1.61. Draine (1989) considered a different data set and suggested an index of 1.75. Recently, Kenyon, Lada, & Barsony (1998) have derived an index of  $1.72_{-0.06}^{+0.07}$  for the  $\rho$  Oph dark cloud. Thus, for  $0.3 \mu\text{m}^{-1} < \lambda^{-1} < 1.1 \mu\text{m}^{-1}$  we employ a power law with index 1.72 normalized to the CCM value at  $\lambda^{-1} = 1.1 \mu\text{m}^{-1}$ . We take the weights  $\sigma_i^{-1} = 1$  for  $1.1 \mu\text{m}^{-1} < \lambda^{-1} < 8 \mu\text{m}^{-1}$  and  $\sigma_i^{-1} = 1/3$  for  $\lambda^{-1} < 1.1 \mu\text{m}^{-1}$  and  $\lambda^{-1} > 8 \mu\text{m}^{-1}$ , since the actual IR extinction is uncertain and the CCM expression for  $\lambda^{-1} > 8 \mu\text{m}^{-1}$  is based on a small number of sight lines.

In Table 2 we list the values of the distribution parameters for which the extinction with  $R_V = 3.1, 4.0,$  and  $5.5$  is best fit, for various values of  $f_g$ . Some of these distributions are displayed in Figure 14. In Table 2 we also report  $\tilde{V}_g$  and  $\tilde{V}_s$ , the total grain volumes in the graphite (including the log-normal contribution) and silicate populations, normalized to their values in the MRN distribution ( $2.67 \times 10^{-27} \text{ cm}^3/\text{H}$  and  $2.79 \times 10^{-27} \text{ cm}^3/\text{H}$ ,

respectively). The MRN volumes are close to the maximum possible values given cosmic abundance constraints; our derived volumes exceed the MRN values by as much as  $\approx 20\%$ . We expect that a model which includes non-spherical grains would produce more extinction per unit grain volume, so we regard our modest violation of cosmic abundance constraints as an artifact due to our use of only spherical grains. We also expect that the total grain volume should not vary substantially from one interstellar environment to another. The lower values for  $\tilde{V}_g$  and  $\tilde{V}_s$  in the fits for  $R_V = 4.0$  and  $5.5$  probably indicate that a significant fraction of the grain mass is locked up in very large grains which have low extinction efficiencies for the range of wavelengths considered.

In Table 2 we also display  $\chi_1^2$  and  $\chi_2^2 = \sum_i (\ln A_{\text{obs}} - \ln A_{\text{mod}})^2$ . Usually the fit is best for  $f_g = 0$ , but hardly suffers as long as  $f_g$  is not too large. In Figure 15 we display  $A_{\text{obs}}$  and  $A_{\text{mod}}$  for  $f_g = 0.0$  and the three values of  $R_V$  in a log-log plot, to give a sense for the fit quality over the entire range of  $\lambda^{-1}$ . In Figures 16, 17, and 18, we display extinction curves for  $f_g = 0$  and for the highest value of  $f_g$  included in Table 2; we show the contribution from each of the grain distribution components.

In assessing the quality of these fits, one must bear in mind that (1) the dielectric functions used are certainly not correct in detail, even for bulk material, (2) the surface monolayers of grains are likely to differ from bulk materials, (3) the true size distributions undoubtedly differ from the adopted functional form, and (4) the interstellar grains are appreciably non-spherical. Therefore, a precise fit is not to be expected. Clearly, extinction data do not well constrain  $f_g$ . Of course, an ideal grain model would employ all of the observational constraints, including IR emission, and a proper treatment of the extinction efficiency for the very small carbonaceous grains, including PAHs.

## 7. Net Photoelectric Heating Rate

In Figure 19 we plot the net total gas heating per H nucleus and per Habing flux,

$$\frac{\Gamma_{\text{tot}}}{G n_{\text{H}}} = \sum_{g,s} \int_{a_{\text{min}}}^{a_{\text{max}}} \frac{\Gamma'_{\text{pe}} - \Lambda'}{G} \frac{1}{n_{\text{H}}} \frac{dn_{\text{gr}}}{da} da \quad (50)$$

as a function of  $G\sqrt{T}/n_e$  for the distributions displayed in Figure 14, with  $T = 100$  K and  $T_c = 3 \times 10^4$  K. The sum is over the graphite and silicate populations. At a single  $G\sqrt{T}/n_e$ , the heating rates obtained for the several distributions span about an order of magnitude, showing the sensitivity of  $\Gamma_{\text{tot}}$  to the grain size distribution. Of course, the highest heating rates are for the distribution with  $R_V = 3.1$  and  $f_g = 0.1$ , which contains the largest population of very small grains. For comparison, we also plot the Bakes & Tielens (1994)

result. Their curve generally lies above our ( $R_V = 3.1$ ,  $f_g = 0.1$ ) curve, primarily because we adopt smaller electron sticking coefficients; this difference is less important for the smallest values of  $G\sqrt{T}/n_e$ . In Figure 20 we show  $\Gamma_{\text{tot}}/Gn_{\text{H}}$  for dust exposed to the ISRF; here we consider typical diffuse cloud dust with  $R_V = 3.1$ , for two possible values of  $f_g = 0$  and 0.1, and gas temperatures of 100 and 6000 K. Note that the net heating when  $T = 100$  K does not differ greatly from that displayed in Figure 19 and that the grains have a net cooling effect for low values of  $G\sqrt{T}/n_e$  when  $T = 6000$  K.

The photoelectric heating rate for the grain size distributions of §6 is fairly well reproduced by the following function:

$$\Gamma_{\text{pe}} \equiv \sum_{g,s} \int_{a_{\text{min}}}^{a_{\text{max}}} \Gamma'_{\text{pe}}(a) \frac{dn_{\text{gr}}}{da} da = 10^{-26} \frac{\text{erg}}{\text{s}} Gn_{\text{H}} \frac{C_0 + C_1 T^{C_4}}{1 + C_2 (G\sqrt{T}/n_e)^{C_5} [1 + C_3 (G\sqrt{T}/n_e)^{C_6}]}, \quad (51)$$

where  $T$  is in K and  $G\sqrt{T}/n_e$  is in  $\text{K}^{1/2} \text{cm}^3$ . Values for the seven parameters in equation (51) are given in Table 3, as well as the largest fractional error,  $\text{err}$ , for  $10 \leq T \leq 10^4$  K and  $10^2 \leq G\sqrt{T}/n_e \leq 10^6 \text{K}^{1/2} \text{cm}^3$ . In general, we consider a blackbody spectrum with  $T_c = 3 \times 10^4$  K; we also consider the ISRF for  $R_V = 3.1$ .

Bakes & Tielens (1994) neglect heating from grains with  $a > 100 \text{Å}$ . This is a good approximation for the highest values of  $G\sqrt{T}/n_e$ , but we find that the heating from larger grains can contribute significantly for low  $G\sqrt{T}/n_e$ . This is demonstrated in Table 3, where we give the fraction  $h_s$  of the total heating due to grains with  $a < 100 \text{Å}$ , for  $G\sqrt{T}/n_e = 10^2 \text{K}^{1/2} \text{cm}^3$  and  $T = 100$  K. For example, for  $R_V = 4.0$ ,  $f_g = 0.03$ , and  $T_c = 3 \times 10^4$  K, 36% of the heating is contributed by grains with  $a > 100 \text{Å}$ . Bakes & Tielens also neglect the heating contributed by silicate grains. We find that silicates contribute  $\lesssim 10\%$  as much heating as graphite when  $G\sqrt{T}/n_e \sim 10^6 \text{K}^{1/2} \text{cm}^3$ . However, the silicate contribution increases as  $G\sqrt{T}/n_e$  decreases, and can reach  $\sim 50\%$  the graphite contribution when  $G\sqrt{T}/n_e \sim 10^2 \text{K}^{1/2} \text{cm}^3$ . (The silicate contribution is more important for lower  $G\sqrt{T}/n_e$  because the silicate population is concentrated at higher  $a$  than the graphite population.) Thus, for relatively bright or warm photodissociation regions (PDRs), large grains and silicates are not important for photoelectric heating. However, for relatively dim and cool PDRs and for the cold and warm diffuse media, with  $G\sqrt{T}/n_e \approx 330$  and 2600, respectively, large grains and silicates could contribute significantly, depending on the size distribution.

The rate of cooling due to charged particle accretion is significant, compared with the photoelectric heating rate, when  $T \gtrsim 10^3$  K. The following approximation is fairly accurate when  $10^3 \leq T \leq 10^4$  K and  $10^2 \leq G\sqrt{T}/n_e \leq 10^6 \text{K}^{1/2} \text{cm}^3$ :

$$\Lambda = 10^{-28} \text{erg cm}^3 \text{s}^{-1} n_e n_{\text{H}} T^{(D_0 + D_1/x)} \exp(D_2 + D_3 x - D_4 x^2) \quad , \quad (52)$$

where  $x = \ln(G\sqrt{T}/n_e)$ . Here  $T$  is in K,  $G\sqrt{T}/n_e$  is in  $\text{K}^{1/2} \text{cm}^3$ , and the values of  $D_i$  are given in Table 4.

## 8. Heating and Cooling in H II Regions

### 8.1. Strömgren Spheres

Lyman continuum radiation from hot stars photoionizes the surrounding gas, resulting in an H II region. Studies of the heating in H II regions have found that photoelectric emission from dust can be important, compared with photoionization of H (Maciel & Pottasch 1982; Oliveira & Maciel 1986; Maloney, Hollenbach, & Townes 1992). In these studies, it was assumed that the photoelectric yield  $Y$  and absorption efficiency factor  $Q_{\text{abs}}$  are independent of grain size and photon energy. Here, we apply our more detailed photoemission model.

In H II regions, the radiation field includes photons with  $h\nu > 13.6 \text{ eV}$ . To see the possible importance of these photons, we calculate integrated photoelectric heating and recombination cooling rates for blackbody spectra with no upper cutoff energy, adopting  $T_c = 3.5 \times 10^4$  and  $4.5 \times 10^4 \text{ K}$ . Of course, at any given location in an H II region, there will be a break in the spectrum at  $13.6 \text{ eV}$ , due in part to absorptions along the path to the star and in part to the break in the stellar spectrum itself. Thus, spectra with no break and with a cutoff at  $13.6 \text{ eV}$  should bracket the range applicable in H II regions.

We take  $n_e/n_H = 1$  and  $T = 9000 \text{ K}$  for the gas. In order to estimate likely  $G/n_H$  values, we consider an O9 V exciting star and a point at the half-mass radius (i.e. at the distance from the star for which half of the H II region volume is enclosed). The radius of the H II region (the “Strömgren radius”) is found by balancing ionizations against recombinations:

$$R_S = \left( \frac{3 \dot{N}_{\text{Ly}}}{4\pi \alpha n_H^2} \right)^{1/3}, \quad (53)$$

where  $\dot{N}_{\text{Ly}}$  is the rate at which the star produces ionizing photons and the case B recombination coefficient  $\alpha \approx 3 \times 10^{-13} \text{ cm}^3 \text{ s}^{-1}$  for gas with  $T \approx 9000 \text{ K}$  (Osterbrock 1989). Since  $R_S \propto n_H^{-2/3}$ ,  $G/n_H \propto n_H^{1/3}$ . We take  $\dot{N}_{\text{Ly}} = 3.63 \times 10^{48} \text{ s}^{-1}$ , luminosity  $L = 4.4 \times 10^{38} \text{ erg s}^{-1}$ , and effective temperature  $T_{\text{eff}} = 3.59 \times 10^4 \text{ K}$  (Vacca, Garmany, & Shull 1996). For  $n_H = 0.1 (10^3) \text{ cm}^{-3}$ ,  $G/n_H \approx 0.5 (10.) \text{ cm}^3$ .

In Tables 5 and 6, we give  $\Gamma_{\text{pe}}/Gn_H$  and  $\Lambda/Gn_H$  for  $G/n_H = 0.1, 1, \text{ and } 10 \text{ cm}^3$ , both with and without the cutoff at  $13.6 \text{ eV}$ , for several of the grain size distributions obtained

in §6. The heating rate increases by factors of several when the cutoff is removed, and the cooling rate is modestly affected, due to changes in the charging. For the spectra with the cutoff, grains have a net cooling effect for all of the considered cases with  $G/n_{\text{H}} = 1.0 \text{ cm}^3$ . For the full spectra, however, we find net heating for all of the cases with  $G/n_{\text{H}} = 1.0 \text{ cm}^3$ . When  $G/n_{\text{H}} < 0.1 \text{ cm}^3$  the grains are negatively charged, so that  $\Gamma_{\text{pe}}/Gn_{\text{H}} \approx \text{constant}$ , and  $\Lambda/Gn_{\text{H}} \propto (G/n_{\text{H}})^{-1}$ , roughly.

The heating rate due to the photoionization of H is approximately

$$\Gamma_{\text{pi}} \sim \alpha n_{\text{H}}^2 k T_{\text{c}} \quad (54)$$

(Osterbrock 1989). Thus, for  $T_{\text{c}} = 3.5 \times 10^4 \text{ K}$ ,

$$\frac{\Gamma_{\text{pi}}}{Gn_{\text{H}}} \sim 1.5 \times 10^{-24} \frac{\text{erg cm}^3}{\text{s}} \left( \frac{G}{n_{\text{H}}} \right)^{-1}. \quad (55)$$

Comparing with the entries in Tables 5 and 6, we find that the net heating from dust can be significant when  $G/n_{\text{H}} \gtrsim 1 \text{ cm}^3$  and can exceed photoionization heating when  $G/n_{\text{H}} = 10 \text{ cm}^3$ .

In an actual H II region, the grain size distribution could be a function of distance from the exciting star, and could differ substantially from those derived in §6. The very small grains might be destroyed in the harsh ionizing environment and the large grains might drift away from the star. A detailed study of the contribution of photoelectric heating in H II regions would have to account for these effects.

## 8.2. The Warm Ionized Medium

The warm ionized medium (WIM), also known as the diffuse ionized gas (DIG), extends to distances above the Galactic midplane  $|z| > 1 \text{ kpc}$  (see Reynolds 1990, 1993 for reviews). It is not yet clear how the WIM is ionized and heated. The only known source of ionization with adequate power to maintain the WIM is Lyman continuum radiation from O stars, but it is not clear how the ionizing photons can reach locations with high  $|z|$ , since atomic gas is highly opaque to these photons. Observed emission line intensity ratios can be approximately reproduced by models in which photoionization by a dilute radiation field dominates (Domgörgen & Mathis 1994). However, such models fail to account for observed variations in line intensity ratios with  $|z|$  (see Reynolds, Haffner, & Tufte 1999 and references therein).

Haffner, Reynolds, & Tufte (1999) found that the line intensity variations could be due to variations in the gas temperature; specifically, they suggested an increase from

$T \approx 7000$  K at  $|z| \approx 500$  pc to  $T \approx 10^4$  K at  $|z| \approx 1500$  pc. Reynolds et al. (1999) noted that the variations are more generally correlated with the electron density, suggesting a supplemental heat source that dominates photoionization heating at low densities. They found that a supplemental heat source  $\Gamma \sim 10^{-25} n_{\text{H}} \text{ erg s}^{-1}$  would result in a temperature profile  $T(|z|)$  which could account for the observed line intensity ratio variations, and suggested photoelectric heating by dust as a possibility.

In Figure 21, we plot the  $T(|z|)$  profile inferred by Reynolds et al. (1999) from observed values of the [N II]/H  $\alpha$  line intensity ratio. In this section we will investigate whether the combination of heating by photoionization and photoemission from dust can reproduce this profile. Reynolds et al. find that the electron density profile can be approximated by

$$n_e(|z|) = 0.125 T_4^{0.45} f^{-0.5} \exp(-|z|/1 \text{ kpc}) \text{ cm}^{-3} \quad , \quad (56)$$

where  $T_4 = T/10^4$  K and  $f$  is the WIM volume filling fraction. Reynolds et al. considered two cases for  $f(|z|)$ :  $f(|z|) = 0.2$  and  $f(|z|) = 0.1 \exp(|z|/0.75 \text{ kpc})$  (Kulkarni & Heiles 1987). We calculate temperature profiles for four different cases, as summarized in Table 7, employing the above two prescriptions for the filling factor and two grain size distributions, for  $R_V = 3.1$  and  $f_g = 0$  and  $0.1$ . We take the heating rate due to photoionization  $\Gamma_{\text{pi}} = 1.0 \times 10^{-24} n_e^2 \text{ erg cm}^3 \text{ s}^{-1}$  and cooling rate (excluding grain collisional cooling)  $\Lambda = 3.0 T_4^{1.9} n_e^2 \text{ erg cm}^2 \text{ s}^{-1}$ , which approximates the cooling function for ionized gas given in Figure 3.2 of Osterbrock (1989).

We plot the temperature profiles for the four cases of Table 7 in Figure 21; we have adjusted the values of  $G$  so that the curves roughly lie on top of the Reynolds et al. curve. In Figure 22, we plot the associated values of the charging parameter  $G\sqrt{T}/n_e$  and the net grain heating  $\Gamma_{\text{tot}}/n_{\text{H}}$  as functions of  $|z|$ ; note that  $\Gamma_{\text{tot}}/n_{\text{H}}$  is not constant, since  $T$  and  $G\sqrt{T}/n_e$  vary with  $|z|$ . For cases A, B, and C, the temperature profiles are too shallow compared with the Reynolds et al. curve. One might expect steeper curves to result if  $G$  is increased, although this might require reducing  $\Gamma_{\text{pi}}/n_e^2$  to unreasonably small values. However, this is not the case, because the photoelectric heating efficiency begins to drop rapidly when  $G\sqrt{T}/n_e \gtrsim 10^3 \text{ K}^{1/2} \text{ cm}^3$ . We can best reproduce the Reynolds et al. temperature profile for case D, with a large population of very small grains and the Kulkarni & Heiles (1987) formula for the WIM filling factor as a function of  $|z|$ . Other heating mechanisms, such as the dissipation of interstellar turbulence (Minter & Spangler 1997), could also contribute, but we see that photoelectric heating by a population of ultrasmall grains appears able to account for the observed temperatures.

## 9. Summary

We have presented a model for photoelectric emission from dust. Here we first summarize how our model differs from the recent study by Bakes & Tielens (1994) and the uncertainties that remain.

We have re-evaluated the photoemission threshold energies for small grains, based in part on an empirical approach employing laboratory data for ionization potentials and electron affinities of PAH molecules. For negatively charged grains, we consider both photoemission from the valence band and the removal of attached electrons, and set the photoemission and photodetachment threshold energies equal to the minimum excitation energy for which an electron can effectively tunnel across the Coulomb barrier. Bakes & Tielens take the emission threshold equal to the electron affinity, which is an underestimate. Motivated by the PAH hypothesis, Bakes & Tielens adopt a disk geometry for the smallest grains. The geometry affects the ionization potential through the capacitance, but this effect is small. We assume spherical grains for simplicity, and thereby retain consistency with the calculation of the charged particle accretion rates  $J_e$  and  $J_{\text{ion}}$ .

We treat the variation of the photoelectric yield with grain charge and the distribution of photoelectron energies in a consistent manner (eq. 12). Whereas Bakes & Tielens adopt a delta function for the distribution of photoelectron energies, we adopt a parabolic form (eq. 11). We adopt a yield function for carbonaceous grains which, like that of Bakes & Tielens, approximately reproduces the measured ionization yield of coronene for grains with  $a \approx 4 \text{ \AA}$ , but which agrees better with experimental determinations of the bulk graphite yield. Still, our bulk yields substantially exceed the experimental results; see the discussion following equation (17). In computing the enhancement factor for the yield of small particles, we evaluate the photon attenuation length  $l_a$  as a function of wavelength (eq. 15), rather than adopting  $l_a = 100 \text{ \AA}$ , independent of wavelength, as Bakes & Tielens do. Recall, however, that the expression for the size-dependent yield enhancement (eq. 14) is based on a simple theoretical model; laboratory investigation of photoemission from microscopic particles is still in its infancy.

Recent experimental results have been used to obtain new estimates for electron sticking efficiencies, as a function of grain size, shown in Figures 6 and 7. We have applied our photoemission and collisional charging model to compute the efficiency with which grains convert absorbed radiation into gas heating via the photoelectric effect, as a function of grain size (§5, Figures 11 – 13). Bakes & Tielens (1994) derived photoelectric heating rates for H I regions by integrating their heating efficiencies over an MRN size distribution with the lower cutoff size for the graphite population extended to  $3.5 \text{ \AA}$ . In §6, we obtain size distributions for graphite-silicate mixtures which reproduce the wavelength-dependent

extinction for  $R_V = 3.1, 4.0,$  and  $5.5$ , with various populations of ultrasmall carbonaceous grains (Figure 14). We integrate the net gas heating rate over these grain size distributions (Figure 19), and we provide fitting functions for the resulting total photoelectric heating and recombination cooling rates (§7). In a separate paper, we will examine the consequences of these revised rates for the thermal structure of the ISM.

Finally, we have applied our model to estimate rates for photoelectric heating by dust grains in H II regions (§8). We find that photoelectric heating by dust can be important in H II regions when  $G/n_H \gtrsim 1 \text{ cm}^3$ . Photoelectric heating in the warm ionized medium (WIM) might explain the observed variations in emission line intensity ratios with distance from the Galactic midplane, if  $\sim 10\%$  of the total carbon is in a population of ultrasmall grains.

We have investigated a range of grain sizes, gas temperatures, radiation field color temperatures, and ratios  $G/n_e$  of radiation intensity to electron density, and selected results have been presented. Interested readers can find a FORTRAN routine that implements the heating and cooling approximations of equations (51) and (52) on the World Wide Web at [www.astro.princeton.edu/~josephw/index.html](http://www.astro.princeton.edu/~josephw/index.html).

This research was supported in part by NSF grant AST-9619429 and by an NSF Graduate Research Fellowship to JCW. We are grateful to R. H. Lupton for the availability of the SM plotting package.

## REFERENCES

- Abouelaziz, H., Gomet, J. C., Pasquerault, D., Rowe, B. R., & Mitchell, J. B. A. 1993, *J. Phys. Chem.*, 99, 237
- Allamandola, L. J., Tielens, A. G. G. M., & Barker, J. R. 1989, *ApJS*, 71, 733
- Bakes, E. L. O. 1992, Ph.D. thesis, Univ. of London
- Bakes, E. L. O., & Tielens, A. G. G. M. 1994, *ApJ*, 427, 822
- Bakes, E. L. O., & Tielens, A. G. G. M. 1995, in *The Diffuse Interstellar Bands*, ed. A. G. G. M. Tielens & T. P. Snow (Dordrecht: Kluwer), 315
- Bohlin, R. C., Savage, B. D., & Drake, J. F. 1978, *ApJ*, 224, 132
- Bohren, C. F. & Huffman, D. R. 1983, *Absorption and Scattering of Light by Small Particles* (New York: Wiley)

- Burtscher, H. & Schmidt-Ott, A. 1982, *Phys. Rev. Lett.*, 48, 1374
- Burtscher, H., Schmidt-Ott, A., & Siegmann, H.C. 1984, *Z. Phys. B*, 56, 197
- Canosa, A., Laubé, S., Rebrion, C., Pasquerault, D., Gomet, J. C., & Rowe, B. R. 1995, *Chem. Phys. Lett.*, 245, 407
- Canosa, A., Parent, D. C., Pasquerault, D., Gomet, J. C., Laubé, S., & Rowe, B. R. 1994, *Chem. Phys. Lett.*, 228, 26
- Cardelli, J. A., Clayton, G. C., & Mathis, J. S. 1989 (CCM), *ApJ*, 345, 245
- Chen, G. D., Ma, S. G., Cooks, R. G., Bronstein, H. E., Best, M. D., & Scott, L. T. 1997, *J. Mass. Spectrom.*, 32, 1305
- Chen, E. S., Chen, E. C. M., Sane, N., Talley, L., Kozanecki, N., & Shulze, S. 1999, *J. Chem. Phys.*, 110, 9319
- Christophorou, L. G., Datskos, P. G., & Faidas, H. 1994, *J. Chem. Phys.*, 101, 6728
- Dartois, E., & d’Hendecourt, L. 1997, *A&A*, 323, 534
- de Jong, T. 1977, *A&A*, 55, 137
- Désert, Boulanger, & Puget 1990, *A&A*, 237, 215
- Domgörgen, H. & Mathis, J. S. 1994, *ApJ*, 428, 647
- Draine, B. T. 1978, *ApJS*, 36, 595
- Draine, B. T. 1989, in *Infrared Spectroscopy in Astronomy*, ed. B. H. Kaldeich (Paris: ESA), 93
- Draine, B. T. & Anderson, N. 1985, *ApJ*, 292, 494
- Draine, B. T. & Lazarian, A. 1998a, *ApJ*, 494, L19
- Draine, B. T. & Lazarian, A. 1998b, *ApJ*, 508, 157
- Draine, B. T. & Lee, H. M. 1984, *ApJ*, 285, 89
- Draine, B. T., & Malhotra, S. 1993, *ApJ*, 414, 632
- Draine, B. T., & Salpeter 1979, *ApJ*, 231, 77
- Draine, B. T., & Sutin, B. 1987, *ApJ*, 320, 803

- Dwek, E. & Smith, R. K. 1996, *ApJ*, 459, 686
- Faraci, G., Pennisi, A. R., & Margaritondo, G. 1989, *Phys. Rev. B*, 40, 4209
- Feuerbacher, B., Anderegg, M., Fitton, B., Laude, L. D., Willis, R. F., & Grard, R. J. L. 1972, *Geochim. Cosmochim. Acta Suppl.* 2, 3, 2655
- Feuerbacher, B. & Fitton, B. 1972, *J. Appl. Phys.* 43, 1563
- Fujihira, M., Hirooka, R., & Inokuchi, H. 1973, *Chem. Phys. Lett.*, 19, 584
- Grevesse, N., Lambert, D. L., Sauval, A. J., van Dishoeck, E. F., Farmer, C. B., & Norton, R. H. 1991, *A&A*, 242, 488
- Guhathakurta, P. & Draine, B. T. 1989, *ApJ*, 345, 230
- Habing, H. J. 1968, *Bull. Astron. Inst. Netherlands*, 19, 421
- Haffner, L. M., Reynolds, R. J., & Tufte, S. L. 1999, *ApJ*, 523, 223
- Huffman, D. R. & Stapp, J. L. 1973, in *IAU Symposium 52, Interstellar Dust and Related Topics*, ed. J. M. Greenberg & H. C. van de Hulst (Dordrecht: Reidel), 297
- Kenyon, S. J., Lada, E. A., & Barsony, M. 1998, *AJ*, 115, 252
- Kim, S.-H. & Martin, P. G. 1995, *ApJ*, 442, 172
- Kulkarni, S. & Heiles C. 1987, in *Interstellar Processes*, ed. D. J. Hollenbach & H. A. Thronson, Jr. (Dordrecht: Reidel), 87
- Lang, N. D. & Kohn, W. 1971, *Phys. Rev. B*, 3, 1215
- Laor, A. & Draine, B. T. 1993, *ApJ*, 402, 441
- Léger, A. & Puget, J. L. 1984, *A&A*, 137, L5
- Lehfaoui, L, Rebrion-Rowe, C., Laubé, S., Mitchell, J. B. A., & Rowe, B. R. 1997, *J. Chem. Phys.*, 106, 5406
- Lias, S. G., et al. 1988, *J. Phys. Chem. Ref. Data*, 17, Suppl. 1
- Lichtenberger, D. L., Nebesny, K. W., Ray, C. D., Huffman, D. R., & Lamb, L. D. 1991, *Chem. Phys. Lett.*, 176, 203
- Lichtenberger, D. L., Rempe, M. E., & Gogosha, S. B. 1992, *Chem. Phys. Lett.*, 198, 454

- Maciel, W. J. & Pottasch, S. R. 1992, *A&A*, 106, 1
- Makov, G., Nitsan, N., & Brus, L. E. 1988, *J. Chem. Phys.*, 88, 5076
- Maloney, P. R., Hollenbach, D. J., & Townes, C. H. 1992, *ApJ*, 401, 559
- Martin, C., Arakawa, E. T., Callcott, T. A., & Warmack, R. J. 1987, *J. Electr. Spectrosc. Rel. Phenom.*, 42, 171
- Mathis, J.S., Mezger, P.G., & Panagia, N. 1983, *A&A*, 128, 212
- Mathis, J. S., Rumpl, W., & Nordsieck, K. H. 1977, *ApJ*, 217, 425
- Mattila, K., Lemke, D., Haikala, L. K., Laureijs, R. J., Léger, A., Lehtinen, K., Leinert, Ch., & Mezger, P. G. 1996, *A&A*, 315, L353
- McFeely, F. R., Cartier, E., Yarmoff, J. A., & Joyce, S. A. 1990, *Phys. Rev. B*, 42, 5191
- Mezger, P.G., Mathis, J.S., & Panagia, N. 1982, *A&A*, 105, 372
- Minter, A. H. & Spangler, S. R. 1997, *ApJ*, 485, 182
- Moskovits, M. 1991, *Ann. Rev. Phys. Chem.*, 42, 465
- Moustefaoui, T., Rebrione-Rowe, C., Le Garrec, J.-L., Rowe, B. R., & Mitchell, J. B. A. 1998, *Faraday Discuss.*, 109, 71
- Müller, U., Schmidt-Ott, A., & Burtscher, H. 1988, *Z. Phys. B*, 73, 103
- Nayak, S. K., Rao, B. K., Khanna, S. N., & Jena, P. 1998, *J. Chem. Phys.*, 109, 1245
- O'Donnell, J. E. 1994, *ApJ*, 422, 158
- Oliveira, S. & Maciel, W. J. 1986, *Ap&SS*, 126, 211
- Onaka, T., Yamamura, I., Tanabé, T., Roellig, T. L., & Yuen, L. 1996, *PASJ*, 48, L59
- Osterbrock, D. E. 1989, *Astrophysics of Gaseous Nebulae and Active Galactic Nuclei* (Mill Valley: University Science Books)
- Press, W. H., Teukolsky, S. A., Vetterling, W. T., & Flannery, B. P. 1992, *Numerical Recipes in FORTRAN: The Art of Scientific Computing, Second Edition* (Cambridge: Cambridge University Press)
- Rebrion-Rowe, C., Lehfaoui, L., Rowe, B. R., & Mitchell, J. B. A. 1998, *J. Chem. Phys.*, 108, 7185

- Reynolds, R. J. 1990, in IAU Symp. 144, The Interstellar Disk/Halo Connection in Galaxies, ed. H. Bloemen (Dordrecht: Kluwer), 67
- Reynolds, R. J. 1993, in Back to the Galaxy, ed. S. S. Holt & F. Verter (A.I.P. Conf. Proc. 278), 156
- Reynolds, R. J., Haffner, L. M., & Tufte, S. L., ApJ, 525, L21
- Rieke, G. H. & Lebofsky, M. J. 1985, ApJ, 288, 618
- Rowe, B. R., Canosa, A., & Le Page, V. 1995, Int. J. Mass Spectroscopy, 149, 573
- Ruoff, R. S., Kadish, R. M., Boulas, P., & Chen, E. C. M. 1995, J. Phys. Chem., 99, 8843
- Schiedt, J., & Weinkauff, R. 1997, Chem. Phys. Lett., 266, 201
- Schmidt-Ott, A., Schurtenberger, P., & Siegmann, H. C. 1980, Phys. Rev. Lett., 45, 1284
- Seidl, M. & Brack, M. 1996, Annals of Physics, 245, 275
- Sellgren, K., 1994, in The Infrared Cirrus and Diffuse Interstellar Clouds, ed. R. Cutri & W. B. Latter, A.S.P. Conference Series, 58, 243
- Smith, D., Spanel, P., & Märk, T. D. 1993, Chem. Phys. Lett., 213, 202
- Spain, I. L. 1973, Chemistry and Physics of Carbon, 8, 1
- Spitzer, L. 1948, ApJ, 107, 6
- Tielens, A. G. G. M., & Hollenbach, D. J. 1985, ApJ, 291, 722
- Tobita, S., Leach, S., Jochims, H. W., Rühl, E., Illenberger, E., & Baumgärtel, H. 1994, Can. J. Phys., 72, 1060
- Tobita, S., Meinke, M., Illenberger, E., Christophourou, L. G., Baumgärtel, H., & Leach, S. 1992, Chem. Phys. 161, 501
- Tosatti, E., & Manini, N. 1994, Chem. Phys. Lett. 223, 61
- Vacca, W. D., Garmany, C. D., & Shull, J. M. 1996, ApJ, 460, 914
- Verstraete, L., Léger, A., d'Hendecourt, L., Dutuit, O., & Défourneau, D. 1990, A&A, 237, 436
- Wang, L.-S., Conceicao, J., Jin, C., & Smalley, R. E. 1991, Chem. Phys. Lett., 182, 5

Wang, L.-S., Desai, S. R., Wu, H., & Nichloas J. B., 1997, *Z. Phys. D*, 40, 36

Wang, X.B., Ding, C.F., & Wang, C.F. 1999, *J. Chem. Phys.*, 110, 8217

Watson, W. D. 1972, *ApJ*, 176, 103

Watson, W. D. 1973, *J. Opt. Soc. Am.*, 63, 164

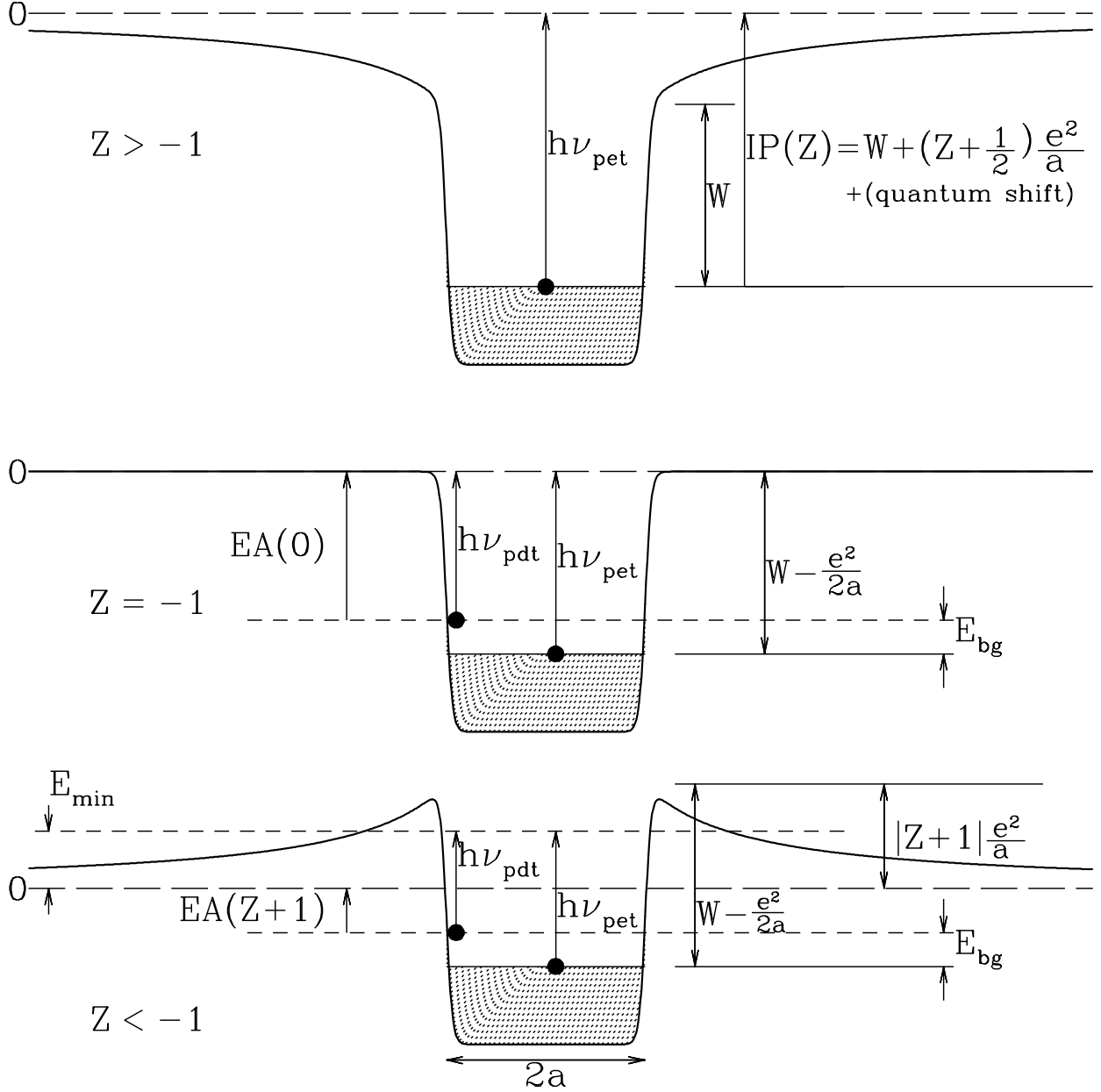


Fig. 1.— Upper panel: The potential confining electrons in a grain with charge  $Ze$ , where  $Z \geq -1$ . Shaded region shows occupied energy levels.  $W$  is the bulk work function, and the photoemission threshold energy  $h\nu_{\text{pet}} = IP$ , the ionization potential. Lower panel: The potential for a grain with  $Z < -1$ . Extra electrons occupy the lowest unoccupied energy level (LUMO) of the neutral grain, lying a distance  $E_A(Z+1)$  below zero, where  $E_A$  is the electron affinity.  $h\nu_{\text{pet}}$  and  $h\nu_{\text{pdt}}$  are the effective threshold energies for photoemission from the valence band and photodetachment, respectively.

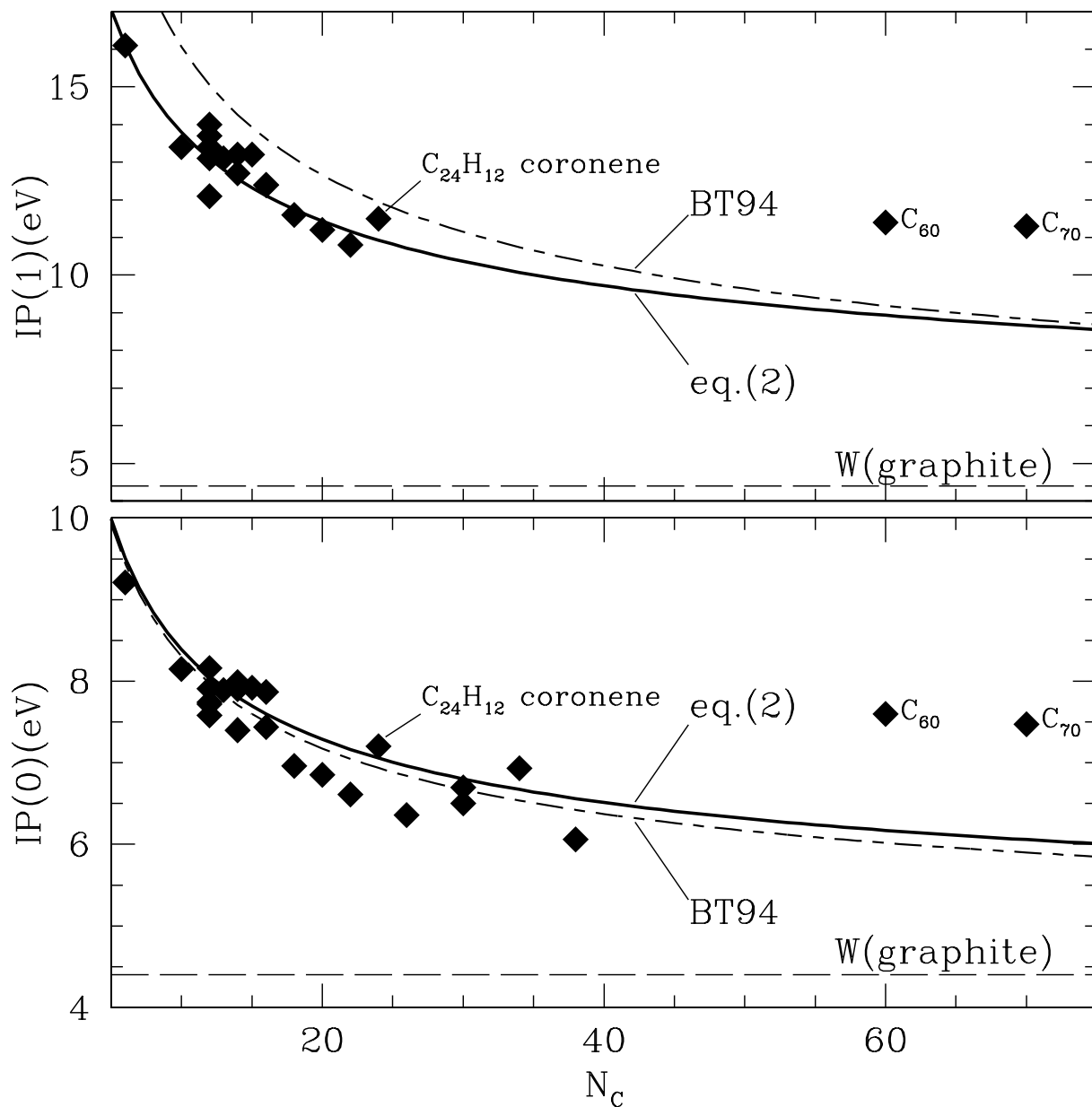


Fig. 2.— First and second ionization potentials  $IP(0)$  and  $IP(1)$  for cyclic aromatic hydrocarbons and fullerenes. Solid curve is eq.(2). Curve labelled BT94 is the  $IP$  estimate of Bakes (1992), used by Bakes & Tielens (1994). Data: Lias et al. (1988) for  $C_{14}H_{10}$  anthracene,  $C_{26}H_{16}$  hexacene,  $C_{30}H_{14}$  dibenz[bc,hl]-coronene,  $C_{30}H_{16}$  pyranthene,  $C_{34}H_{18}$  tetrabenz[a,cdj,lm]-perylene; Tobita et al. (1994) for  $C_{10}H_8$  naphthalene,  $C_{12}H_8$  biphenylene,  $C_{12}H_8$  acenaphthylene,  $C_{12}H_{10}$  biphenyl,  $C_{12}H_{10}$  acenaphthene,  $C_{12}H_{10}$  2-vinylnaphthalene,  $C_{13}H_{10}$  fluorene,  $C_{14}H_{10}$  diphenylacetylene,  $C_{14}H_{12}$  9,10-dihydrophenanthrene,  $C_{14}H_9N$  acridine,  $C_{16}H_{10}$  pyrene  $C_{16}H_{10}$  fluoranthene,  $C_{18}H_{12}$  tetracene,  $C_{20}H_{12}$  perylene,  $C_{22}H_{14}$  pentacene,  $C_{24}H_{12}$  coronene; Chen et al. (1999) for  $C_{38}H_{20}$  benz[42]; Lichtenberger et al. (1991), Lichtenberger et al. (1992), and Steger et al. (1992) for  $C_{60}$ ,  $C_{70}$  fullerenes.

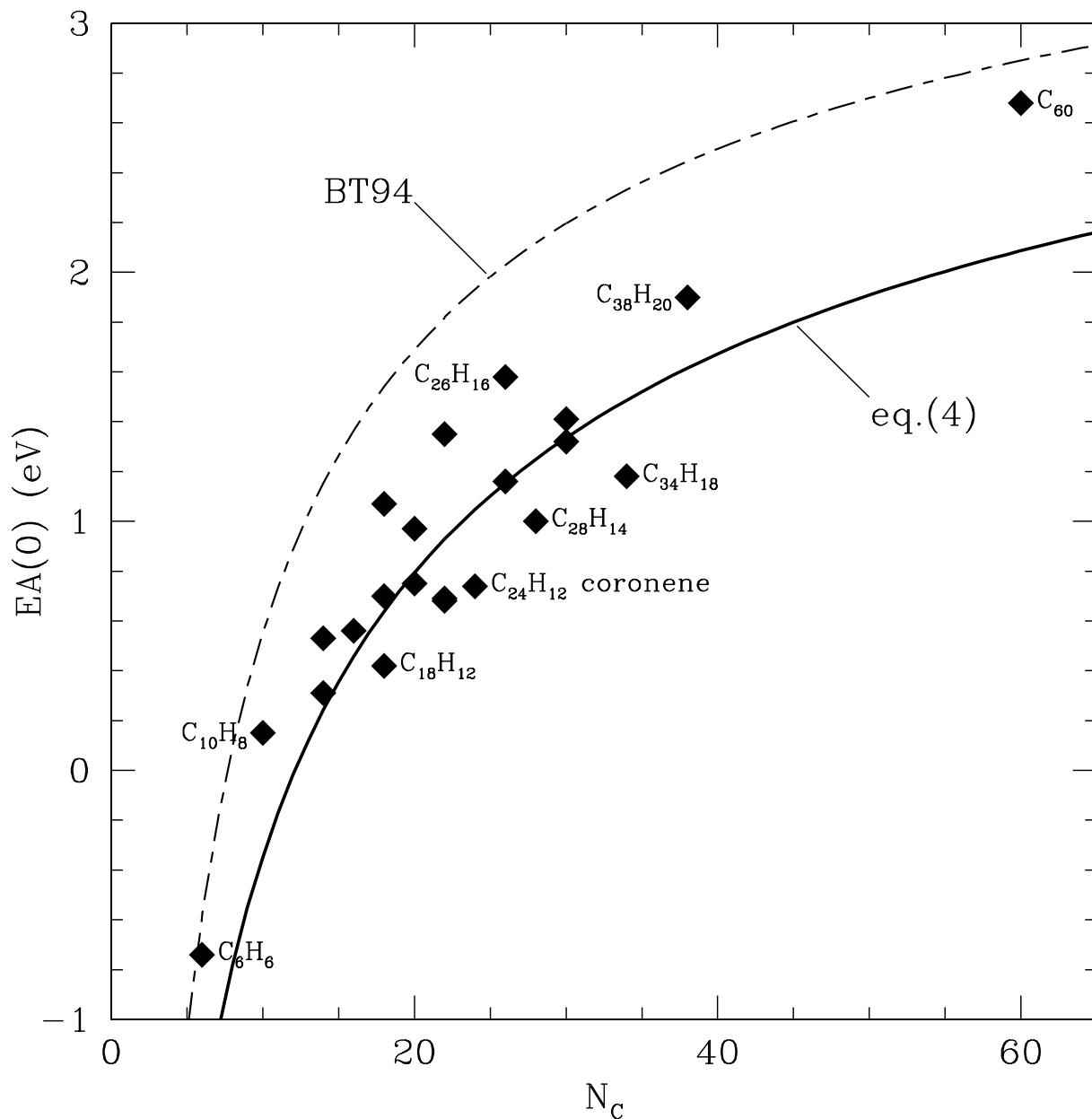


Fig. 3.— Electron affinity for neutral PAH molecules and  $C_{60}$ . Solid curve is eq.(4). Curve labelled BT94 is estimate of Bakes (1992), used by Bakes & Tielens (1994). Data: Chen et al (1999) for  $C_6H_6$  benzene,  $C_{24}H_{12}$  coronene,  $C_{26}H_{16}$  hexacene,  $C_{30}H_{14}$  dibenz[bc,hl]-coronene,  $C_{30}H_{16}$  pyranthene,  $C_{34}H_{18}$  tetrabenz[a,cdj,lm]-perylene,  $C_{38}H_{20}$  benz[42]; Shiedt & Weinkauff (1997) for  $C_{14}H_{10}$  anthracene; Ruoff et al. (1995) for  $C_{10}H_8$  naphthalene,  $C_{14}H_{10}$  phenanthrene,  $C_{16}H_{10}$  pyrene,  $C_{18}H_{12}$  tetracene,  $C_{18}H_{12}$  benzanthracene,  $C_{18}H_{12}$  chrysene,  $C_{20}H_{12}$  perylene,  $C_{20}H_{12}$  benzo(a)pyrene,  $C_{22}H_{14}$  pentacene,  $C_{22}H_{14}$  dibenz(a,j)anthracene; Chen et al. (1997) for  $C_{26}H_{12}$  diindenochrysene,  $C_{28}H_{14}$  debenzo[a,g]corannulene; and Wang, Ding, & Wang (1999) for  $C_{60}$  fullerene.

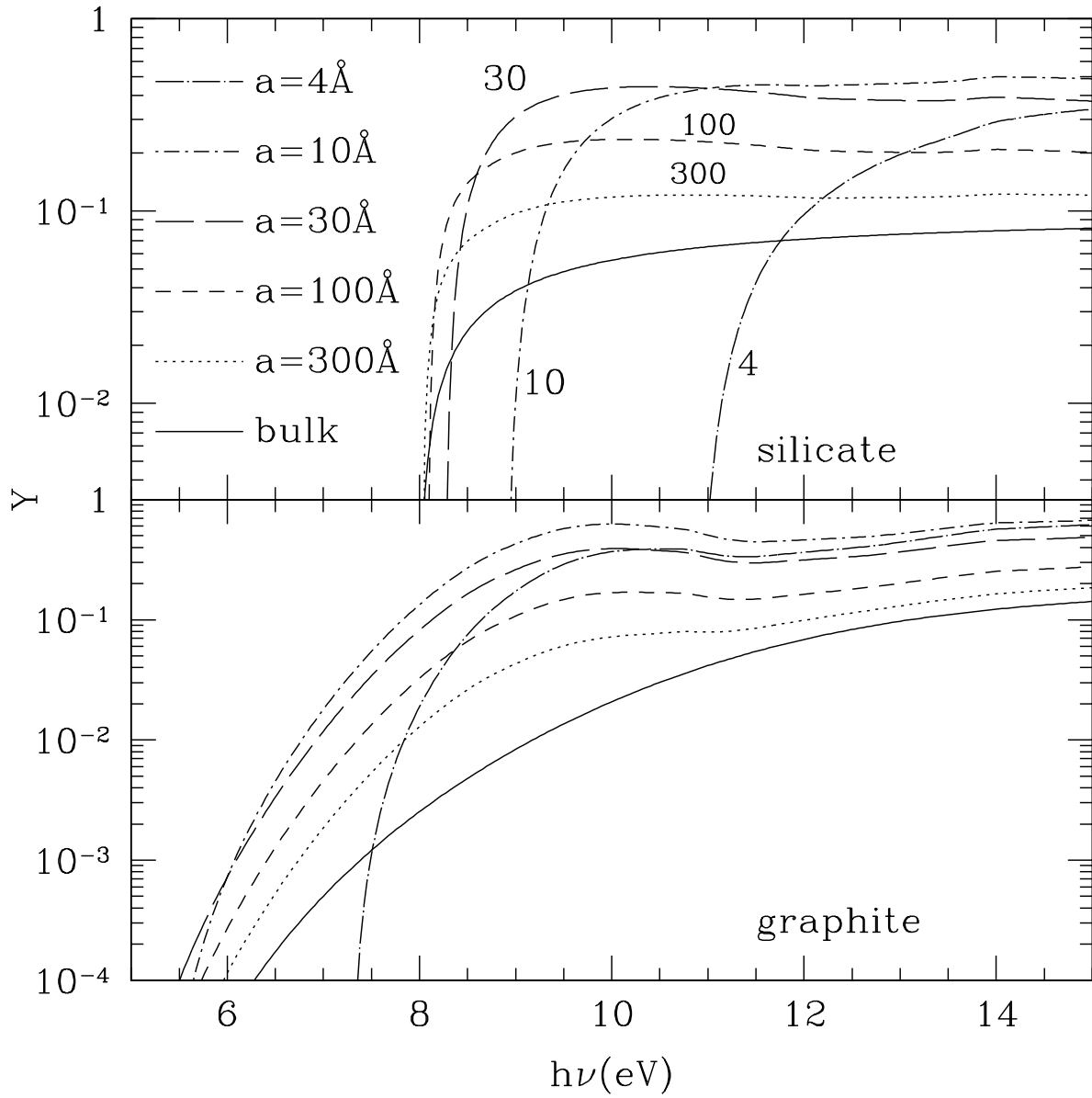


Fig. 4.— Photoelectric yield  $Y$  for neutral graphite and silicate grains as a function of incident photon energy  $h\nu$ , for several values of the grain size  $a$ , as indicated.

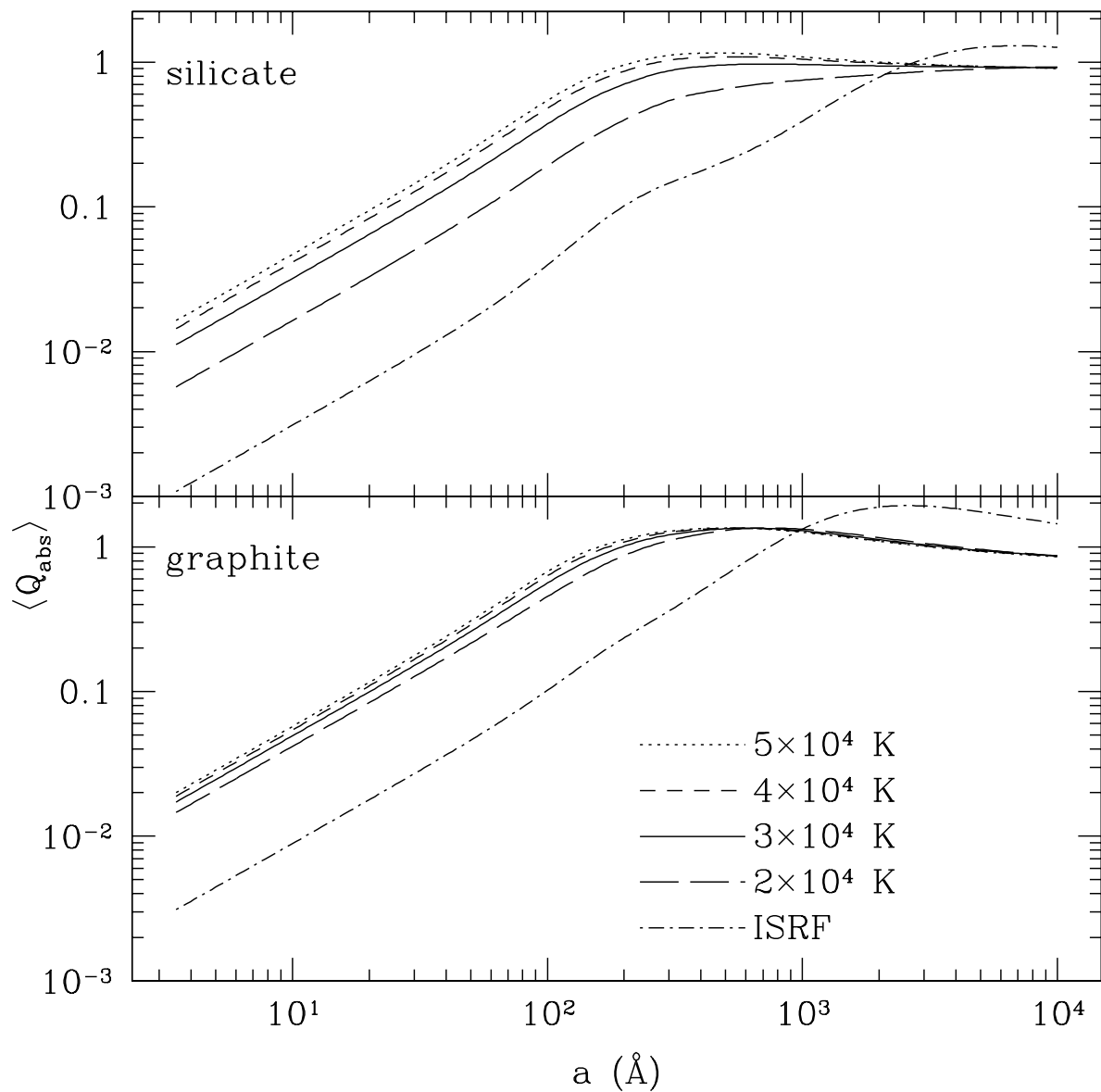


Fig. 5.— Absorption efficiency factors for graphite and silicate grains, averaged over the interstellar radiation field (ISRF) and blackbody spectra with indicated color temperatures.

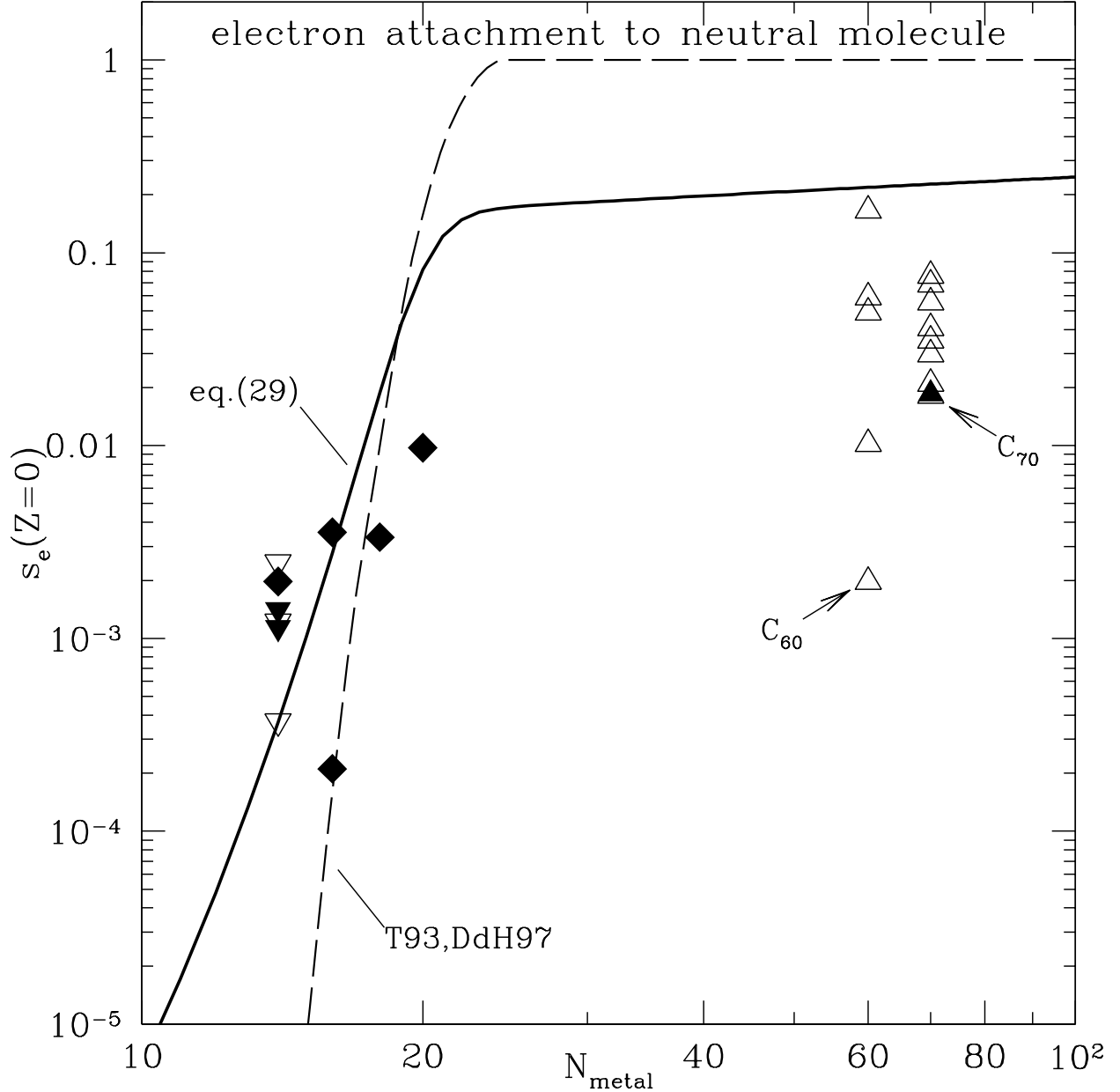


Fig. 6.— Sticking coefficients  $s_e$  for electron attachment to neutral molecules, as a function of  $N_{\text{metal}}$ , the number of atoms other than H. Diamonds: acridine  $C_{13}H_9N$ , fluoranthene  $C_{16}H_{10}$ , pyrene  $C_{16}H_{10}$ , tetracene  $C_{18}H_{12}$ , and perylene  $C_{20}H_{12}$  (Tobita et al. 1992). Triangles: anthracene  $C_{14}H_{10}$  (Tobita et al. 1992; Canosa et al. 1994; Moustefaoui et al. 1998),  $C_{60}$  (Smith et al. 1993), and  $C_{70}$  (Spanel & Smith 1994). Filled symbols are for  $T = 300\text{K}$ . Open symbols for  $C_{60}$  and  $C_{70}$  are for  $T = 500 - 4500\text{K}$ . Open symbols for anthracene are for  $T = 48 - 170\text{K}$  (Moustefaoui et al. 1998). Solid curve: adopted empirical fit given by eq. (29). Broken curve:  $s_e$  adopted by Tielens (1993) and Dartois & d’Hendecourt (1997).

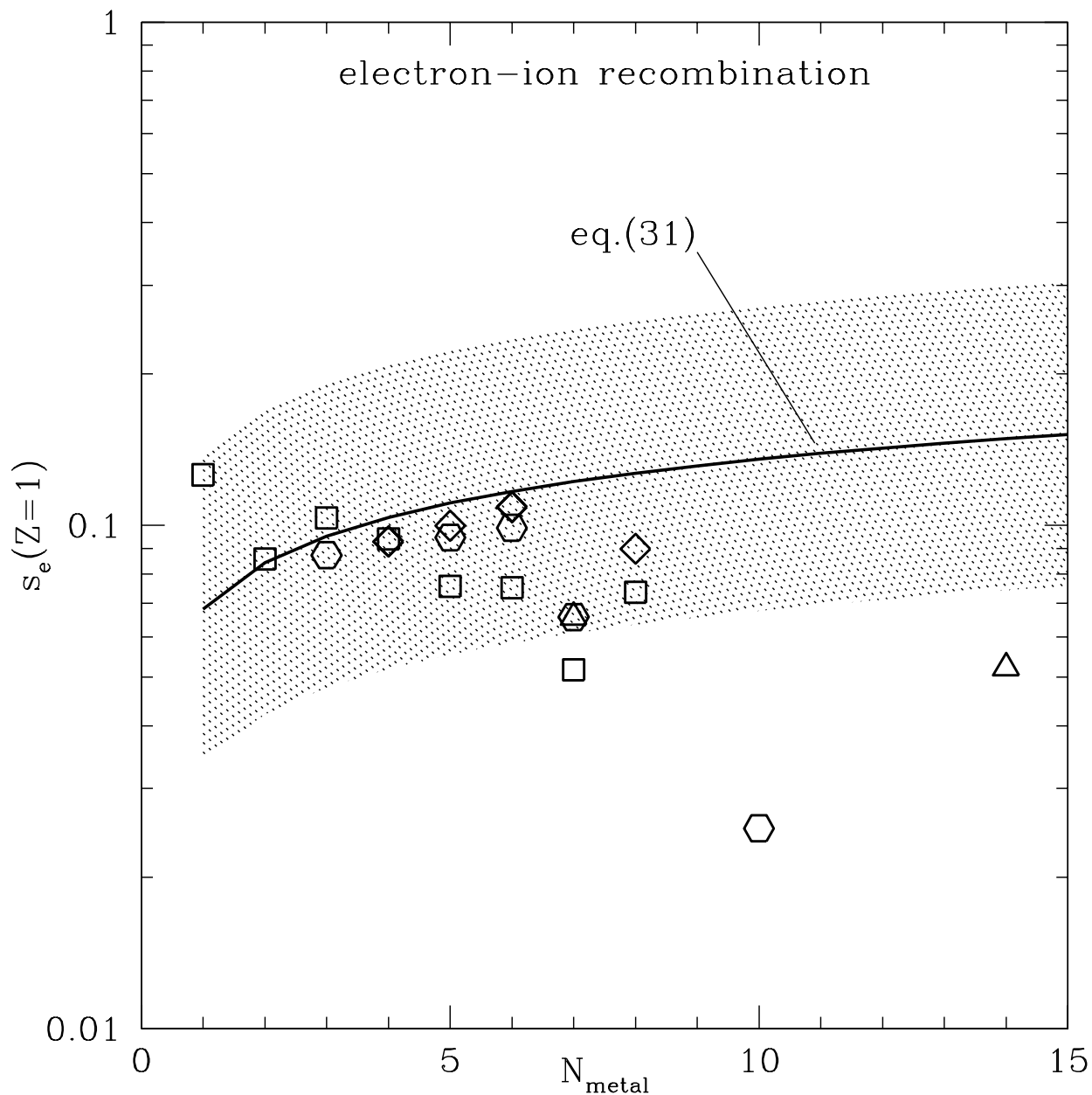


Fig. 7.— Sticking coefficients  $s_e$  for electron recombination with positive ions. Hexagons:  $T = 300\text{K}$  experimental results of Abouelaziz et al. (1993) for  $\text{C}_3\text{H}_3^+$ ,  $\text{C}_5\text{H}_3^+$ ,  $\text{C}_6\text{H}_6^+$ ,  $\text{C}_7\text{H}_5^+$ , and  $\text{C}_{10}\text{H}_8^+$ . Squares:  $T = 300\text{K}$  results of Lehfaoui et al. (1997) for alkanes  $\text{CH}_5^+$ ,  $\text{C}_2\text{H}_5^+$ ,  $\text{C}_3\text{H}_7^+$ ,  $\text{C}_4\text{H}_9^+$ ,  $\text{C}_5\text{H}_{11}^+$ ,  $\text{C}_6\text{H}_{13}^+$ ,  $\text{C}_7\text{H}_{15}^+$ , and  $\text{C}_8\text{H}_{17}^+$ . Triangle:  $T = 300\text{K}$  results of Rowe et al. (1995) for  $\text{C}_7\text{H}_8^+$  and  $\text{C}_{14}\text{H}_{10}^+$  phenanthrene. Diamonds:  $T = 300\text{K}$  results of Rebrion-Rowe et al. (1998) for  $\text{C}_4\text{H}_5^+$ ,  $\text{C}_4\text{H}_{11}^+$ ,  $\text{C}_5\text{H}_9^+$ ,  $\text{C}_6\text{H}_4^+$ ,  $\text{C}_6\text{H}_5^+$ ,  $\text{C}_8\text{H}_7^+$ . Solid curve: adopted empirical fit given by eq. (31); shaded region is within factor of two of empirical fit.

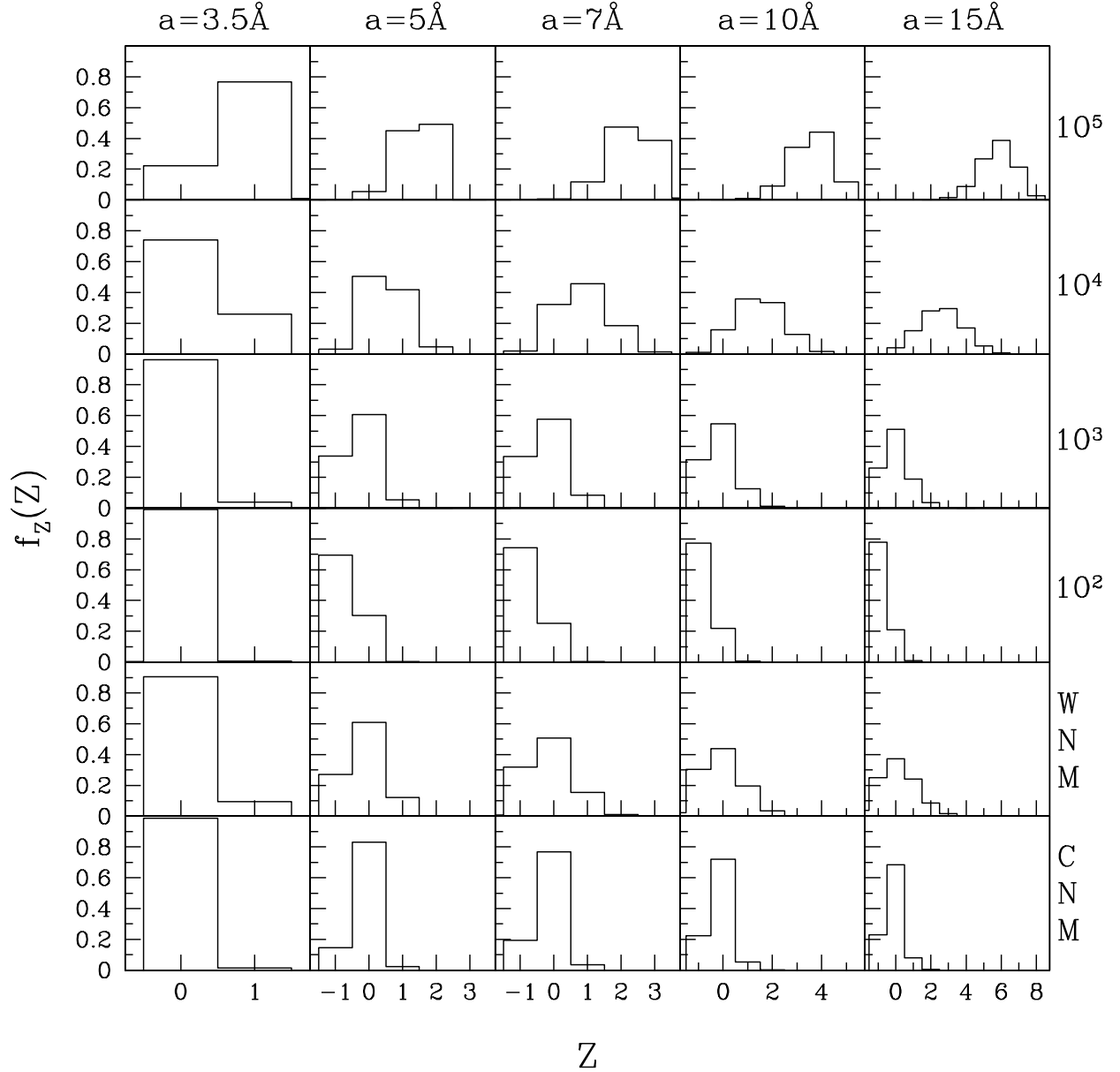


Fig. 8.— Charge distributions for graphite grains with  $a = 3.5, 5, 7, 10,$  and  $15\text{\AA}$  and six sets of ambient conditions. For the upper four panels, we adopt a blackbody radiation spectrum (cut off at  $13.6\text{ eV}$ ) with  $T_c = 3 \times 10^4\text{ K}$  and  $T = 10^3\text{ K}$ ; the values of  $G\sqrt{T}/n_e$ , in  $\text{K}^{1/2}\text{ cm}^3$  are indicated. The bottom two panels are for the warm neutral medium (WNM) and cold neutral medium (CNM).

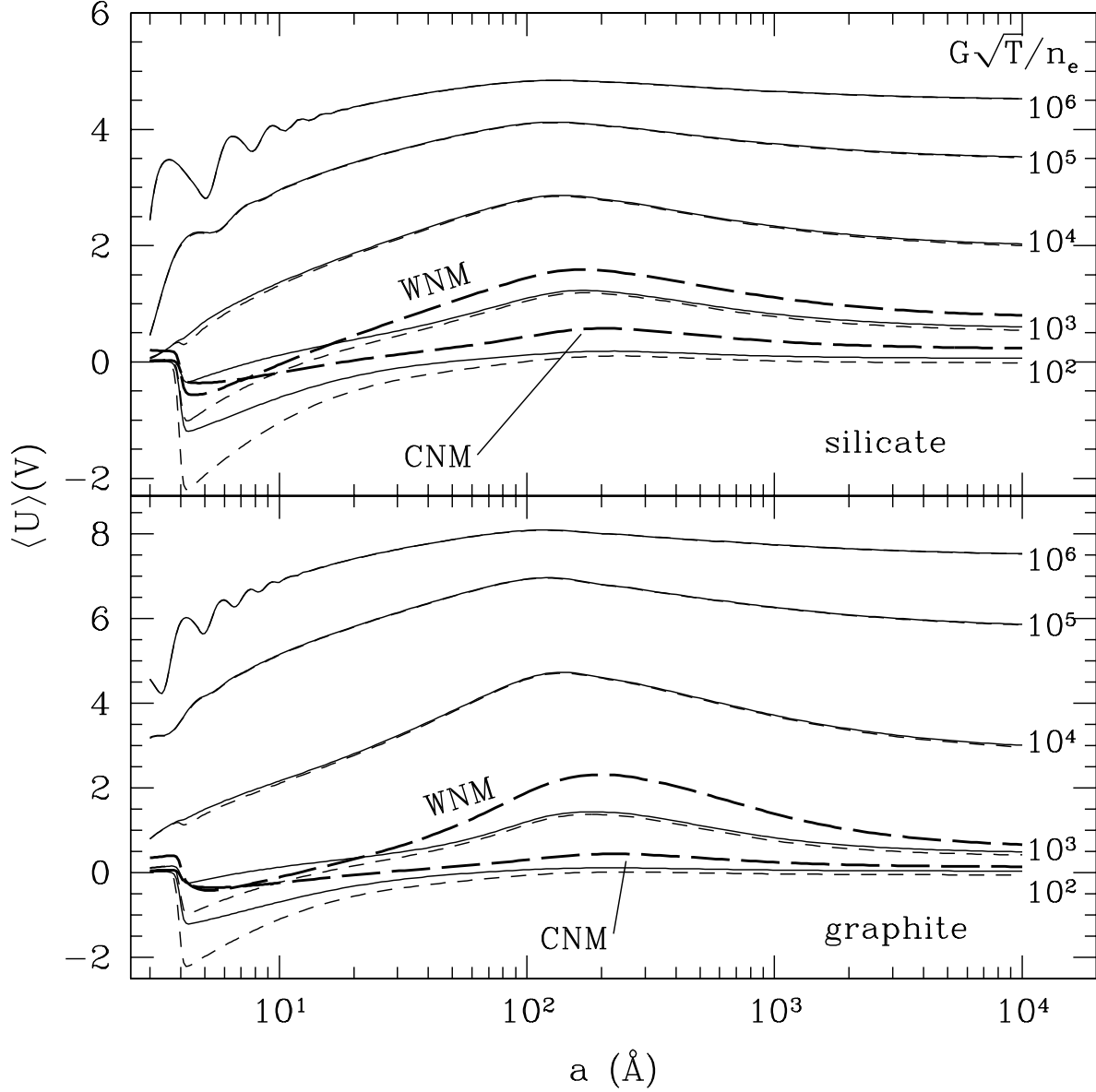


Fig. 9.— Average electrostatic potential  $\langle U \rangle$  for  $T_c = 3 \times 10^4$  K. The top (bottom) panel is for silicate (graphite) grains; curves labelled CNM (WNM) are for cold (warm) neutral media; solid (short-dashed) lines indicate  $T = 100$  K (1000 K). For the  $T = 100$  K and 1000 K curves, values of  $G\sqrt{T}/n_e$  are indicated in  $\text{K}^{1/2} \text{cm}^3$ .

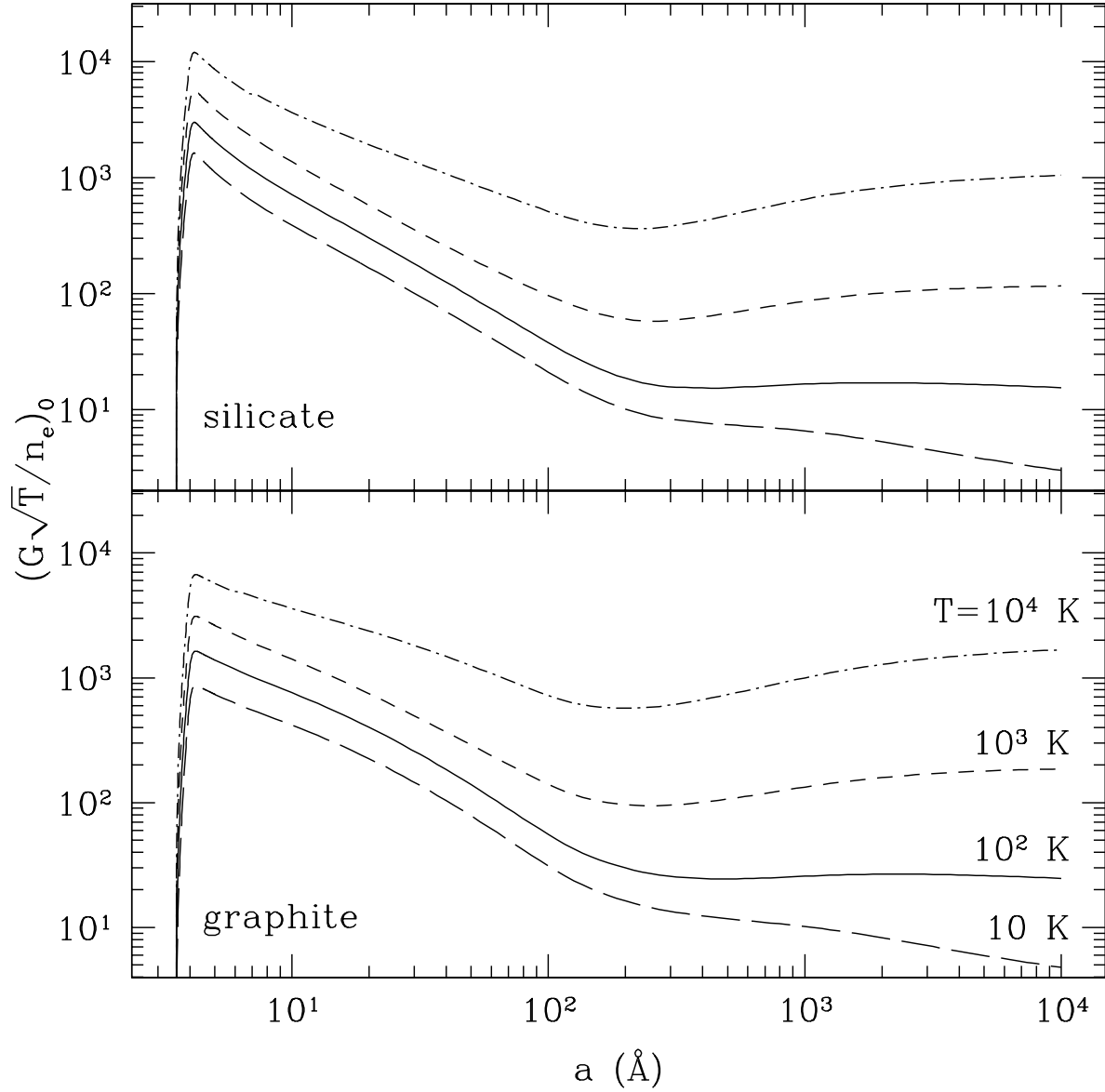


Fig. 10.— The value of the charging parameter for which  $\langle Z \rangle = 0$ , for graphite and silicate grains, a blackbody radiation field with  $T_c = 3 \times 10^4$  K, and various gas temperatures, as labeled.

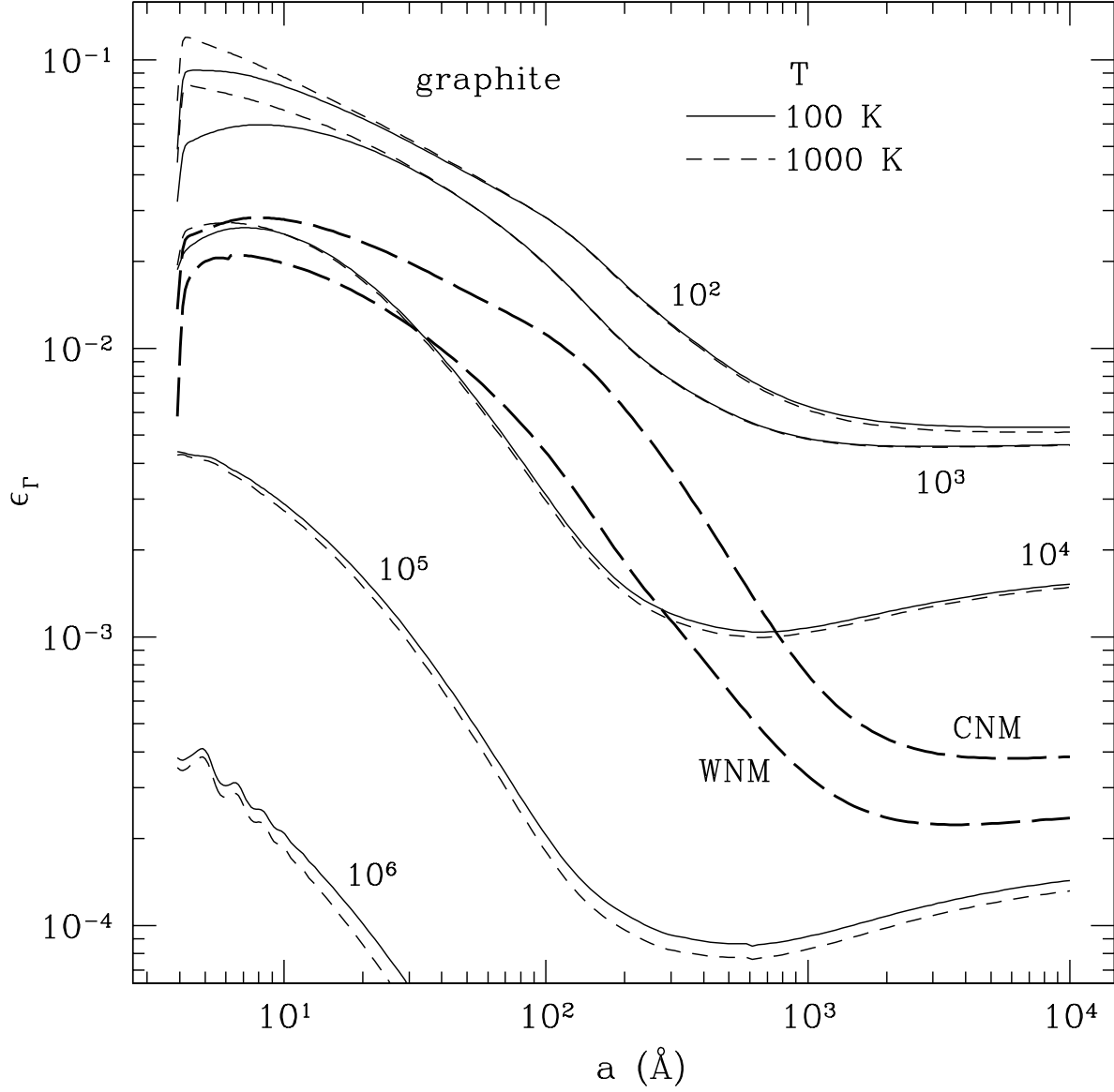


Fig. 11.— Gas heating efficiency for graphite grains for two gas temperatures: 100 K (solid) and  $10^3$  K (short-dashed), four values of  $G\sqrt{T}/n_e$ , as labelled, and  $T_c = 3 \times 10^4$  K. Curves labelled CNM (WNM) are for cold (warm) neutral media and the ISRF.

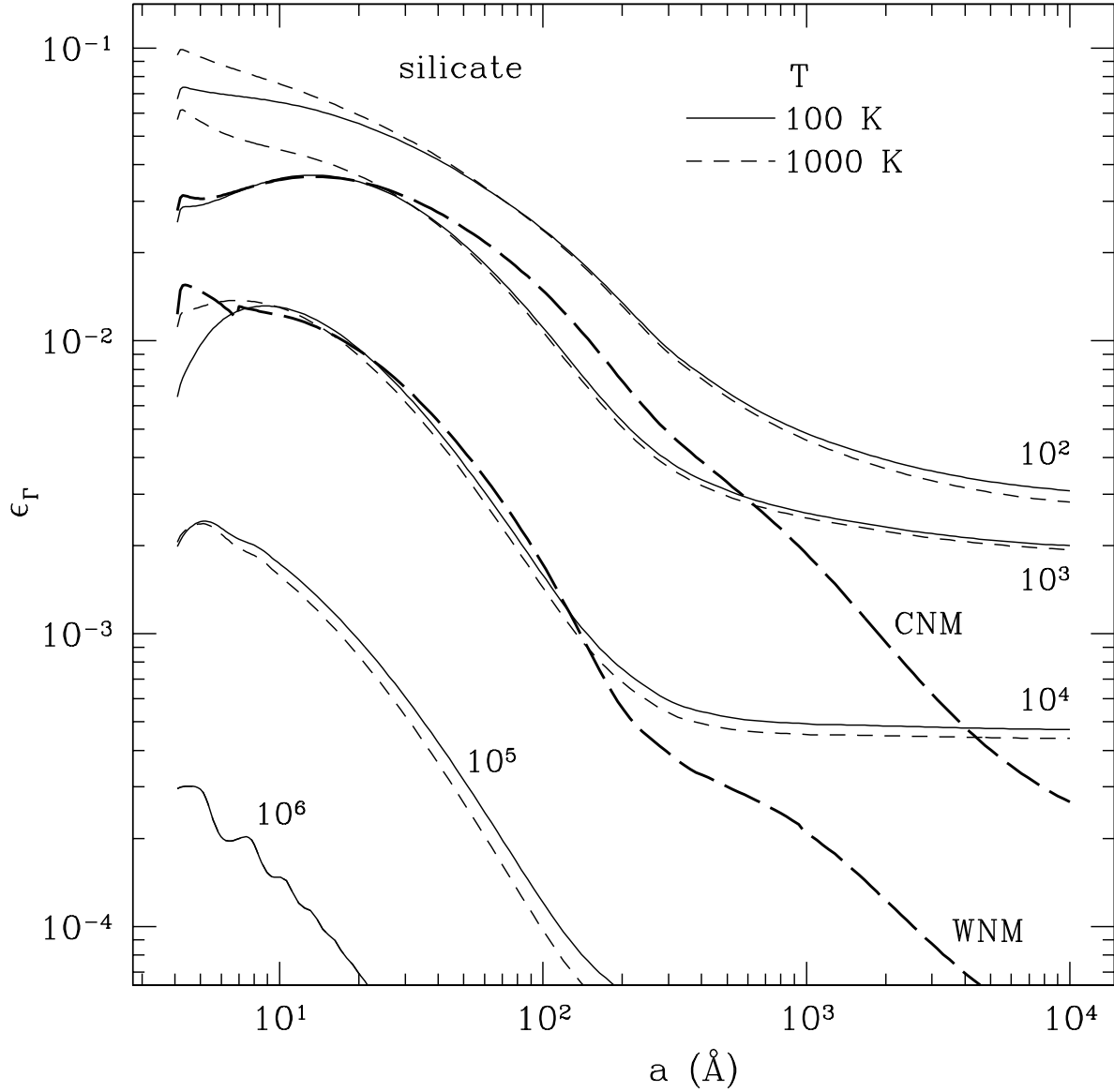


Fig. 12.— Same as Figure 11, but for silicate grains. The curve for  $T = 1000$  K and  $G\sqrt{T}/n_e = 10^6 \text{ K}^{1/2} \text{ cm}^3$  lies entirely below the plot region.

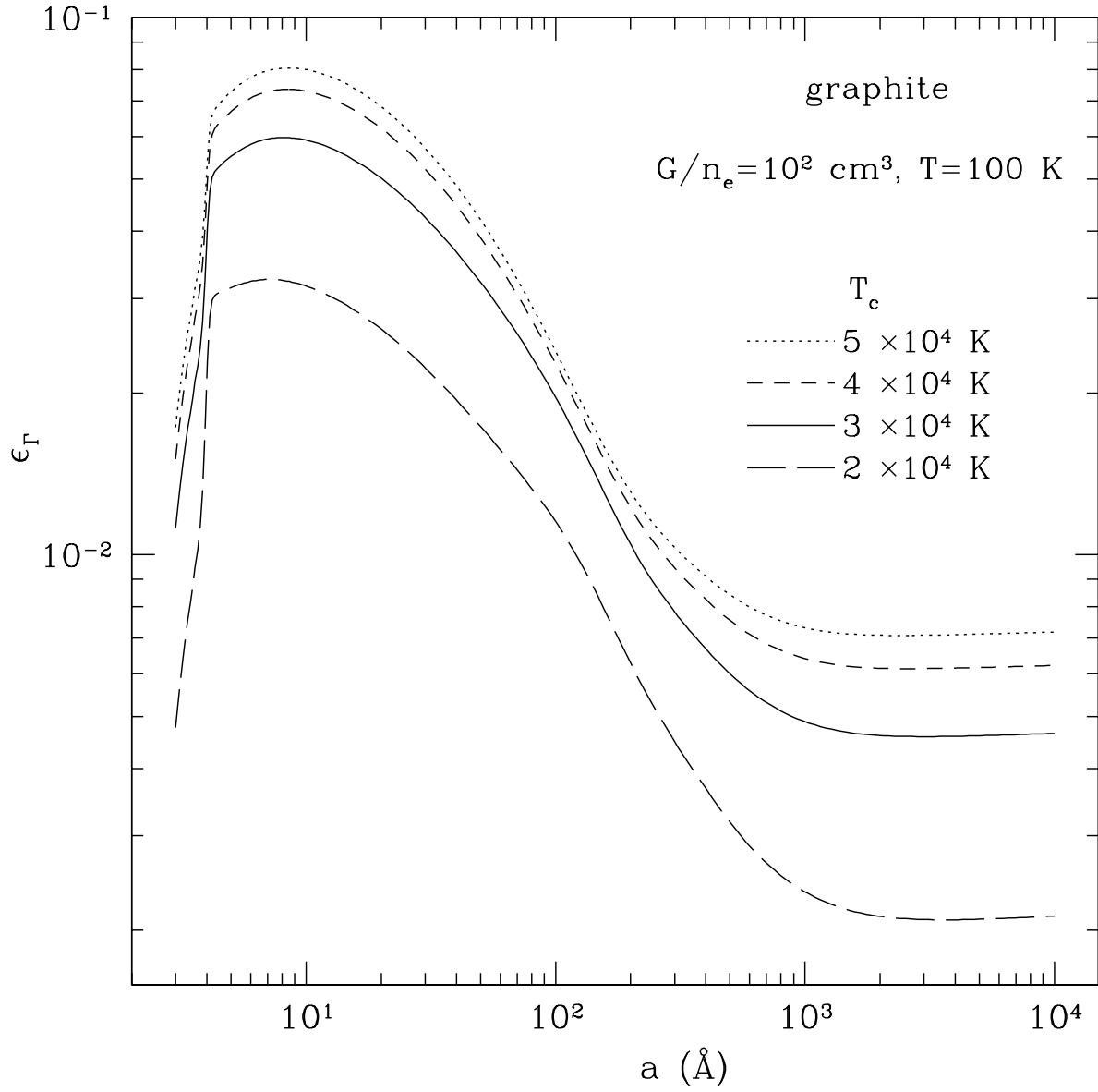


Fig. 13.— Gas heating efficiency for graphite grains,  $T = 100 \text{ K}$ ,  $G\sqrt{T}/n_e = 10^3 \text{ K}^{1/2} \text{ cm}^3$ , and four values of  $T_c$  as indicated.

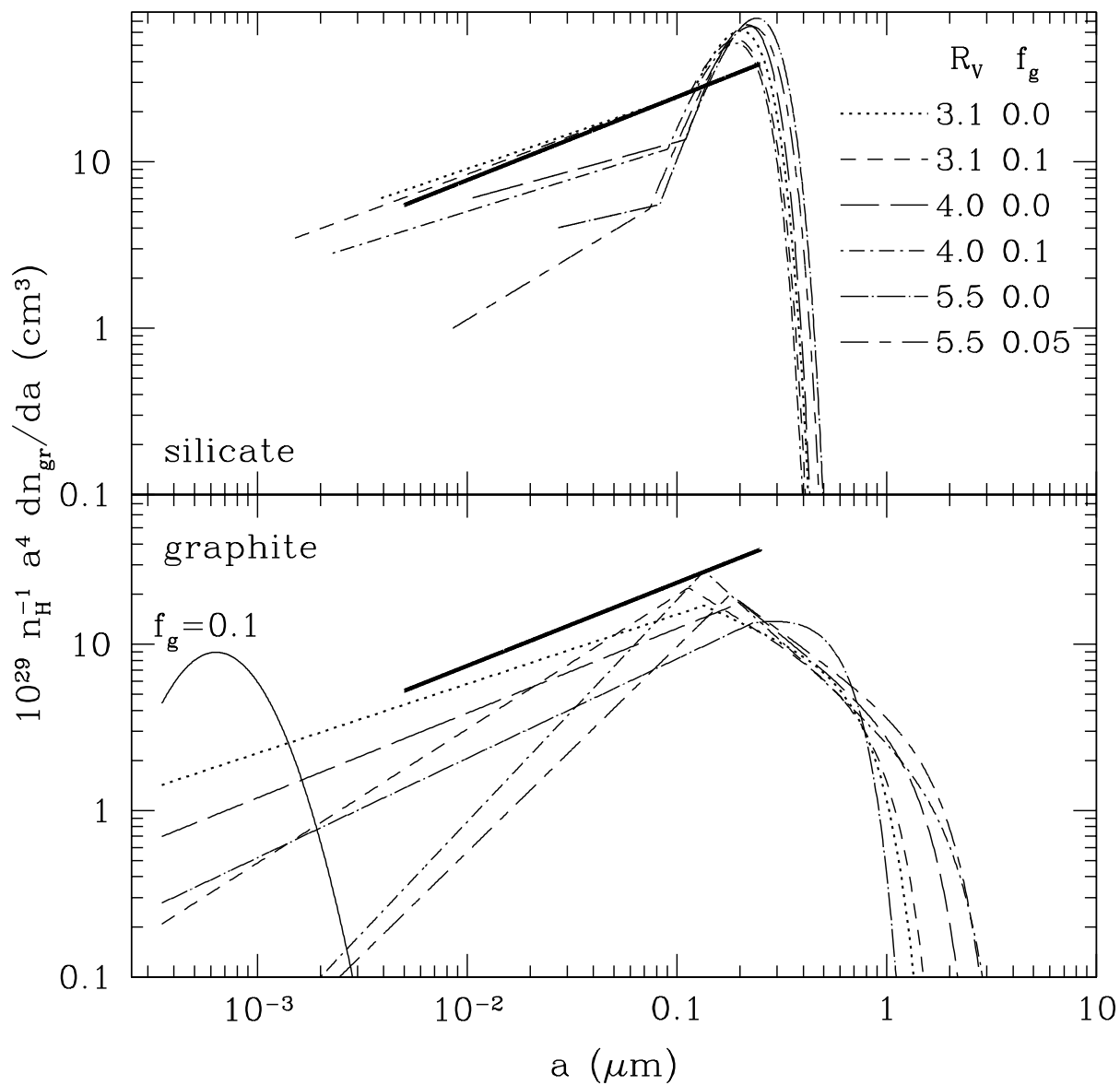


Fig. 14.— Grain size distributions. The values of  $R_V$ ,  $f_g$  are indicated. The log-normal graphite contribution is not included for each case; the solid curve labelled  $f_g = 0.1$  is for the log-normal population (eq. 45) with  $f_g = 0.1$ . The heavy, solid lines are the MRN distribution, for comparison.

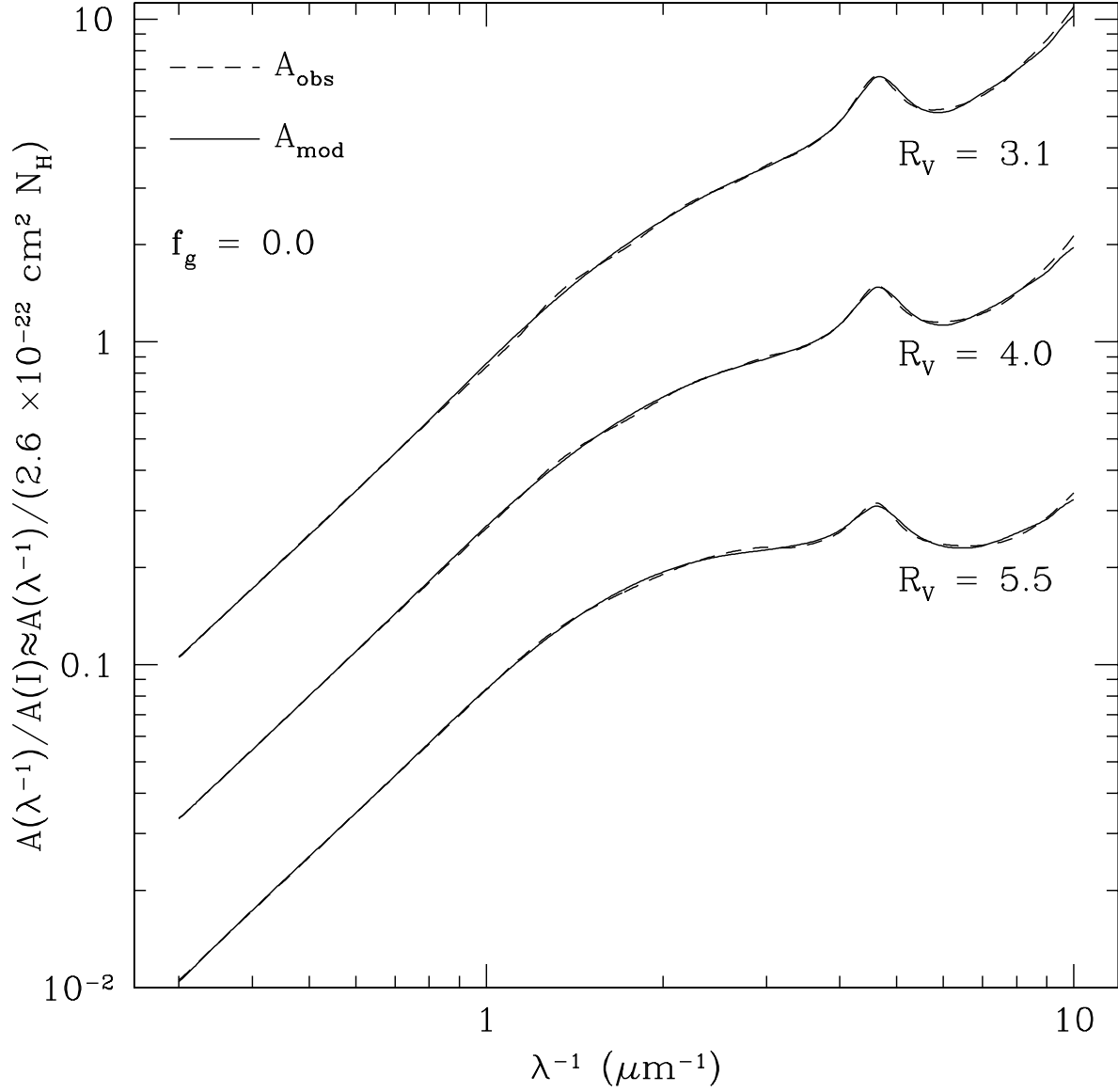


Fig. 15.— The average “observed” extinction  $A_{\text{obs}}$  and the extinction resulting from our models with  $f_g = 0.0$ . The curves for  $R_V = 4.0$  ( $5.5$ ) are scaled down by a factor  $10^{0.5}$  ( $10$ ), for clarity.

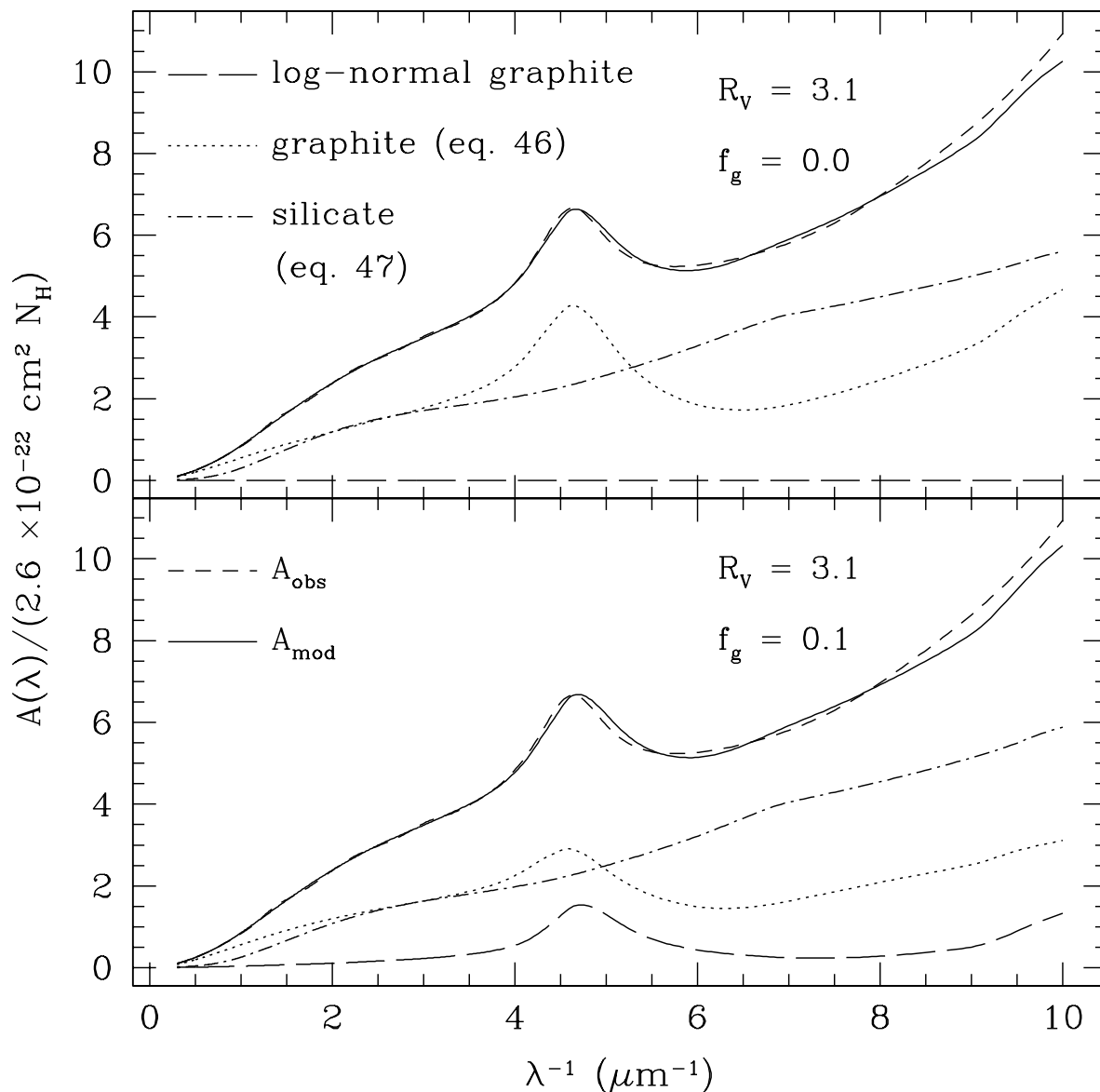


Fig. 16.— The extinction curve  $A_{\text{mod}}$  resulting from the grain distribution of equations (47) and (48), with parameters optimized to fit  $A_{\text{obs}}$  (see text) for  $R_V = 3.1$  (also shown), for  $f_g = 0.0$  and 0.1. The contributions from the three grain distribution components are also shown.

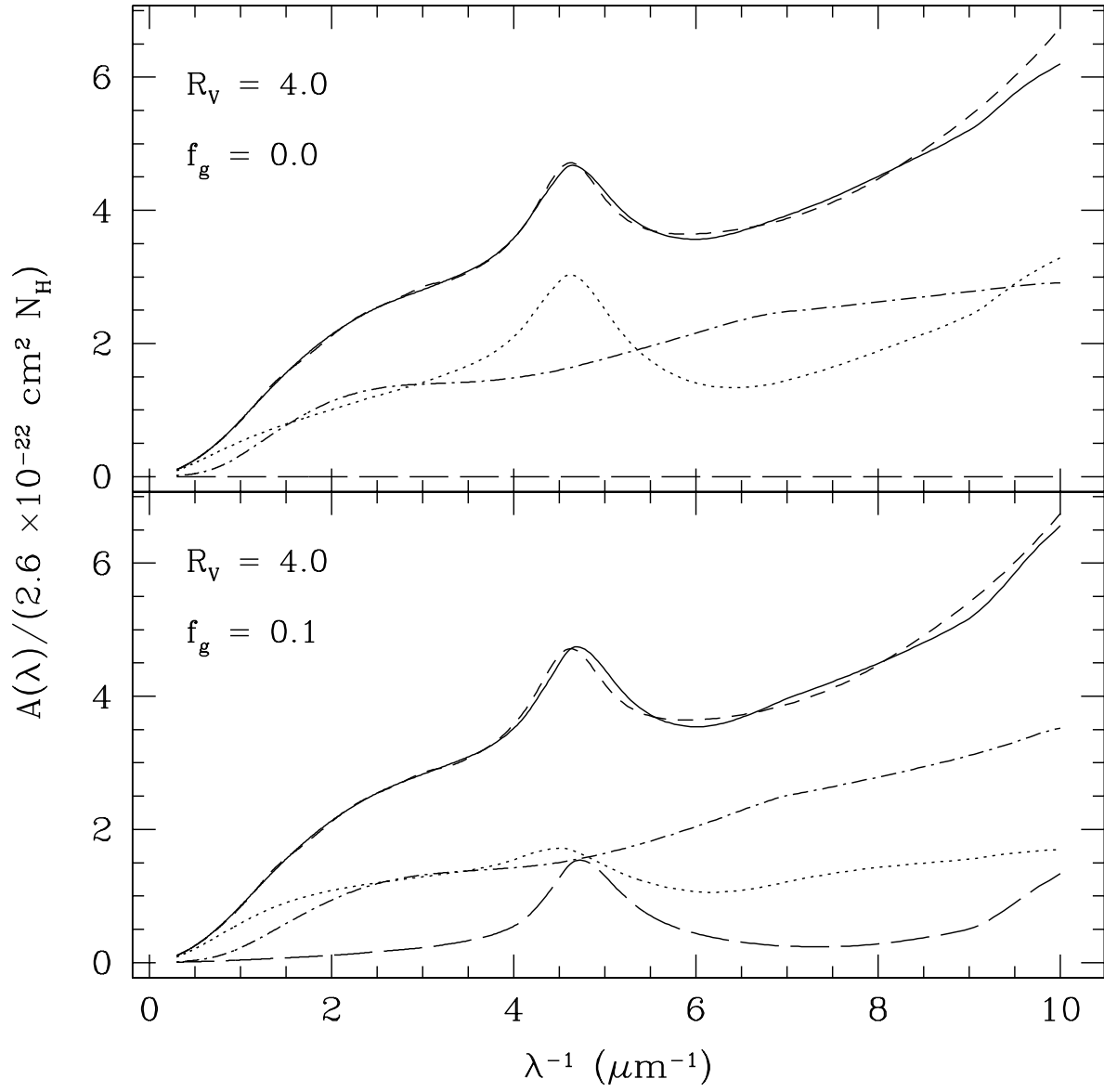


Fig. 17.— Same as Figure 16, but for  $R_V = 4.0$  and  $f_g = 0.0$  and  $0.1$ .

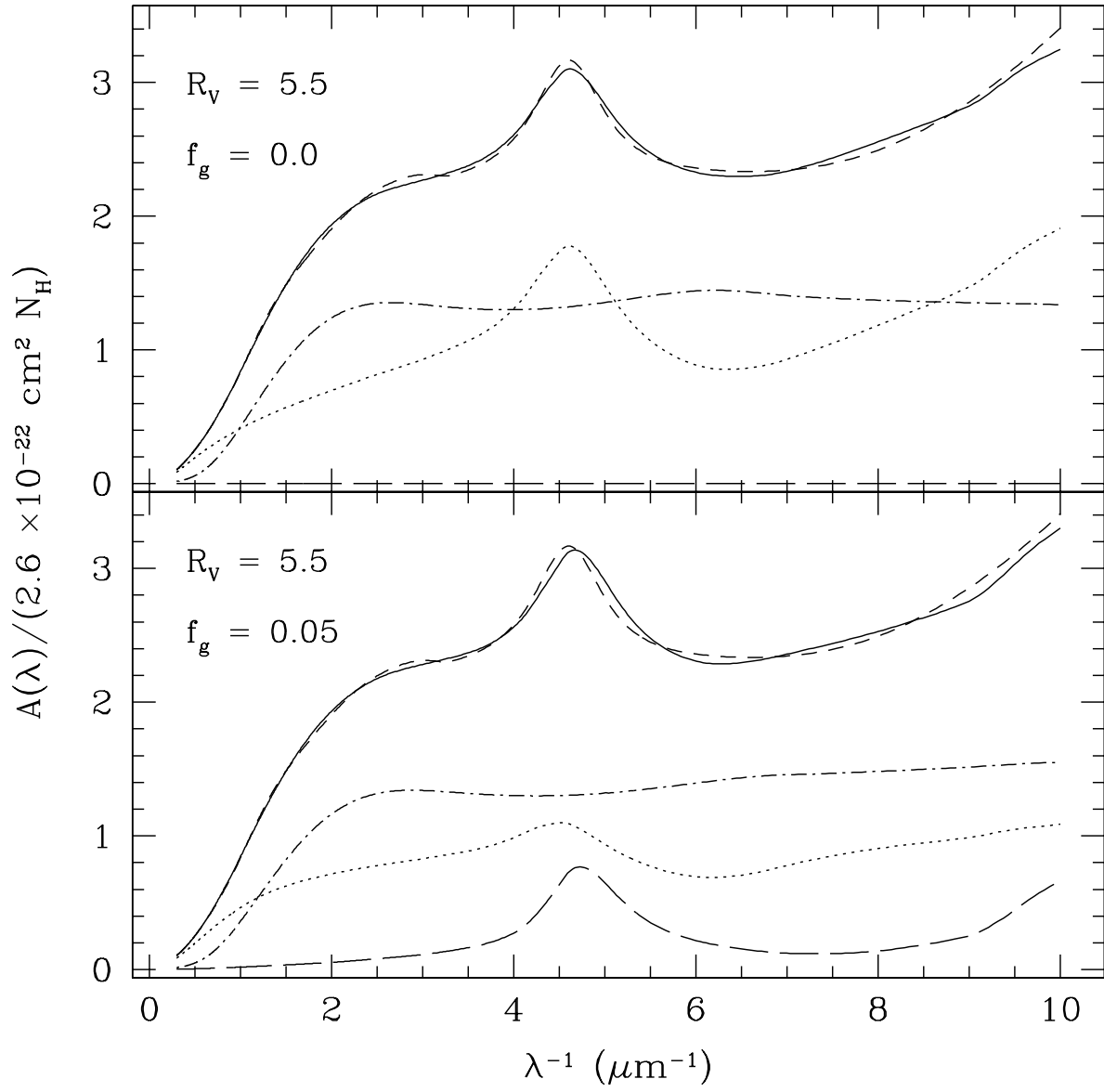


Fig. 18.— Same as Figure 16, but for  $R_V = 5.5$  and  $f_g = 0.0$  and  $0.05$ .

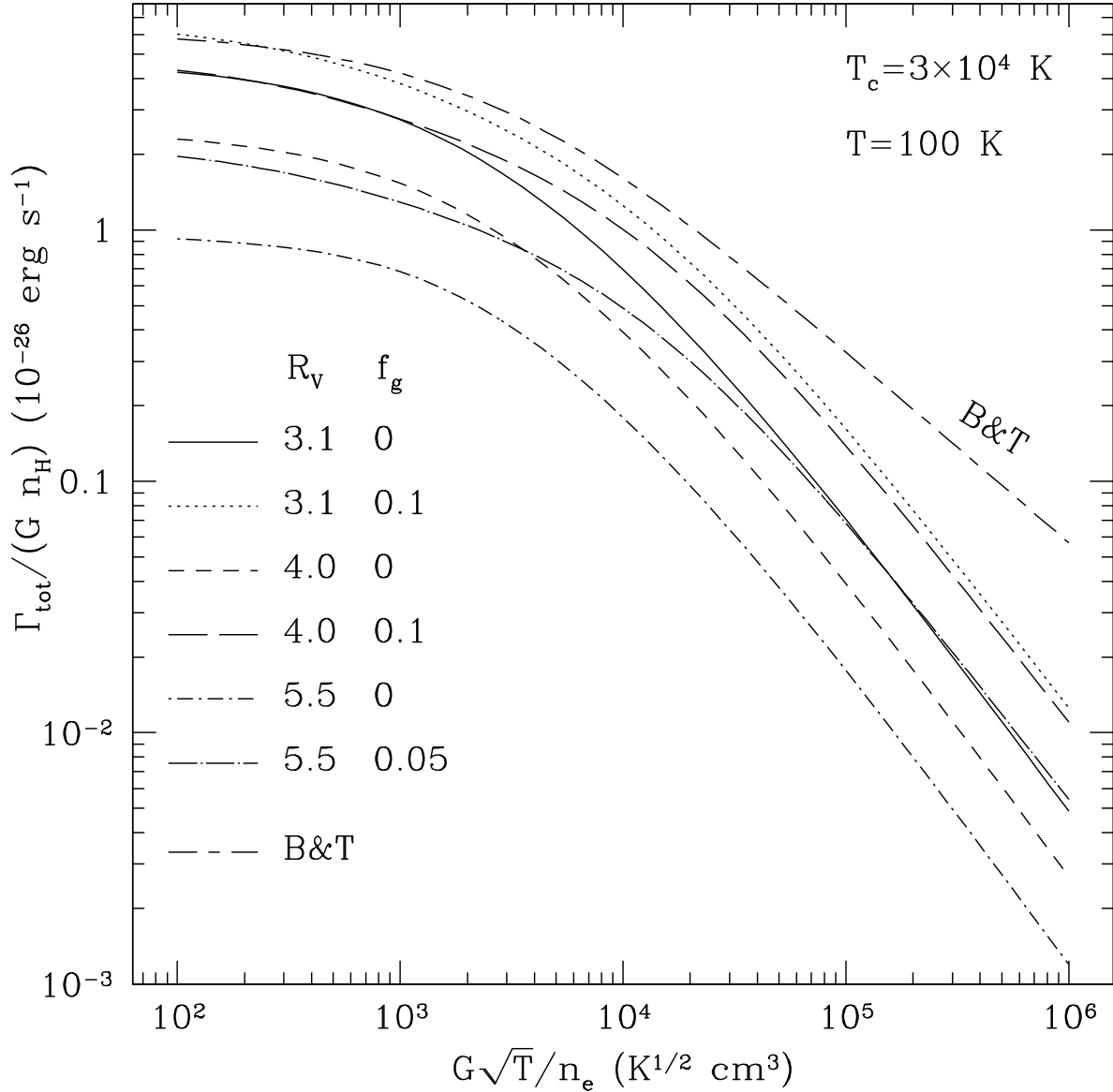


Fig. 19.— The photoelectric heating rate minus the cooling rate due to gas phase ions and electrons colliding with and sticking to the grains; for radiation color temperature of  $3 \times 10^4 \text{ K}$ , gas temperature of  $100 \text{ K}$ , and grain size distributions derived in §6 for various values of  $R_V$  and  $f_g$ . For comparison, we also display the Bakes & Tielens (1994) result (B & T).

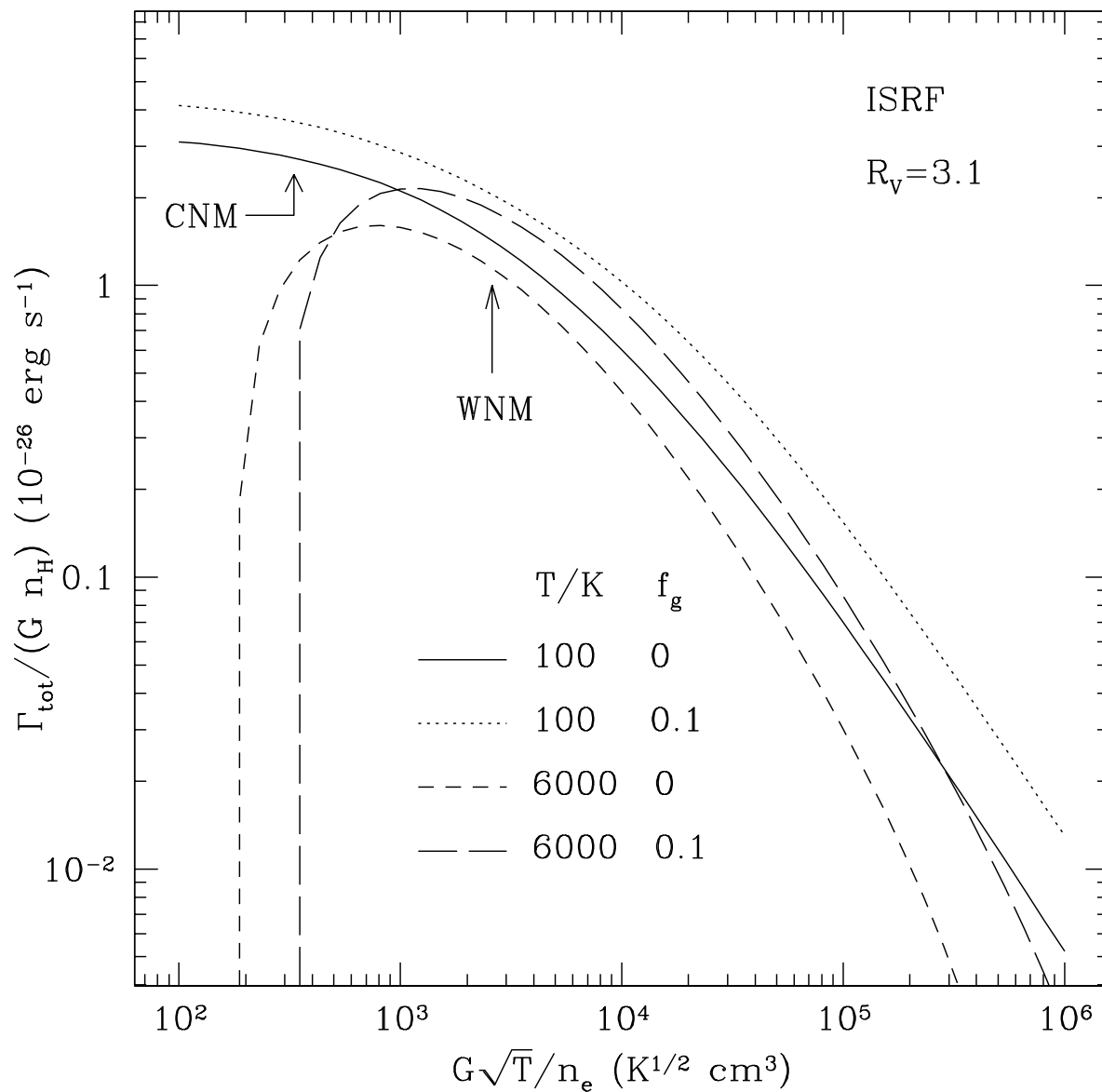


Fig. 20.— Same as Figure 19, but for the ISRF of equation (32),  $R_V = 3.1$ , and various values of  $f_g$  and gas temperature  $T$ .

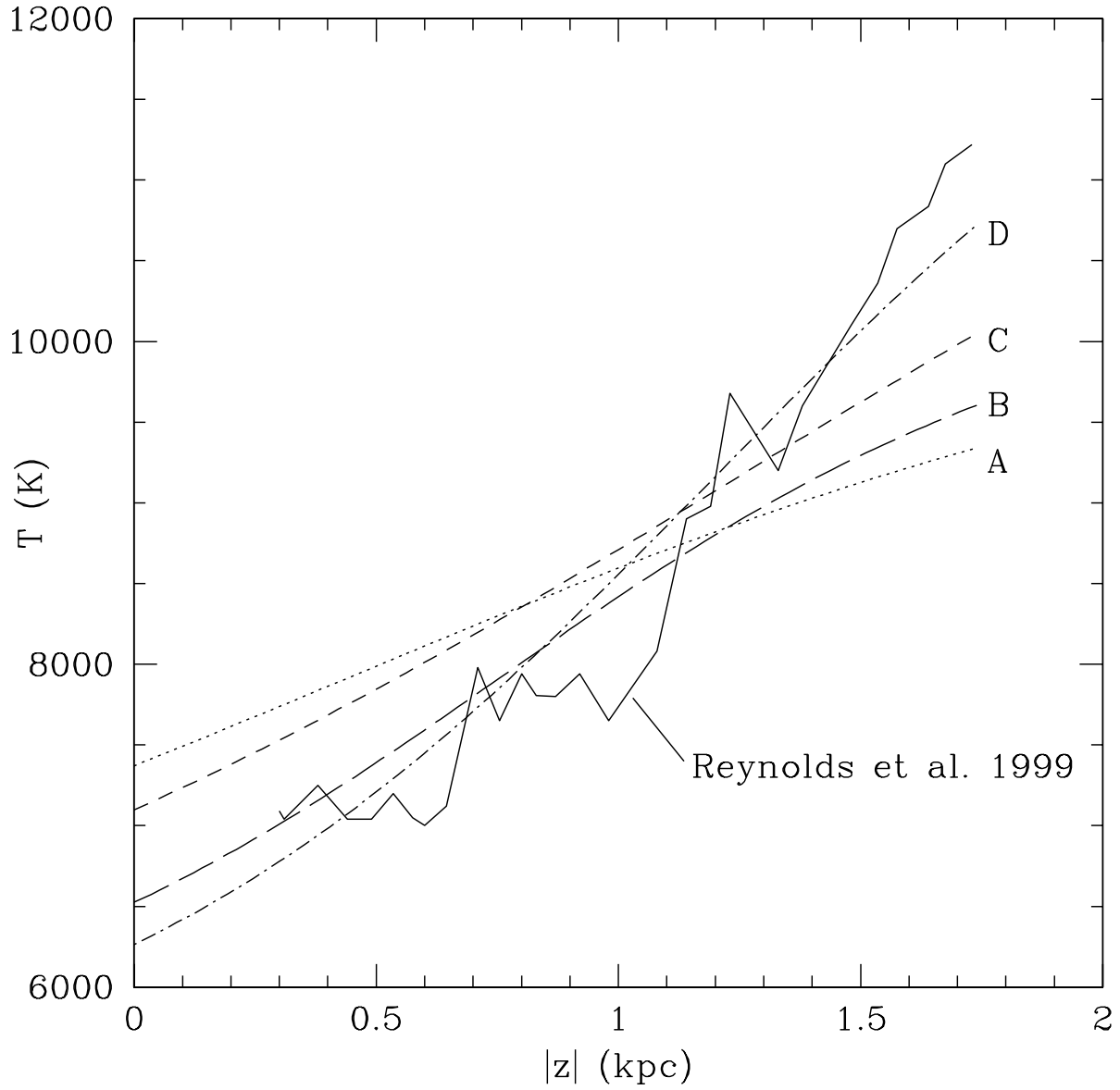


Fig. 21.— WIM temperature profiles as a function of distance from the Galactic midplane  $|z|$ . The solid curve was inferred by Reynolds et al. (1999) from observations of the  $[\text{N II}]/\text{H } \alpha$  line intensity ratio; the other curves are results of calculations including photoelectric heating, for various sets of parameter values as indicated in Table 7.

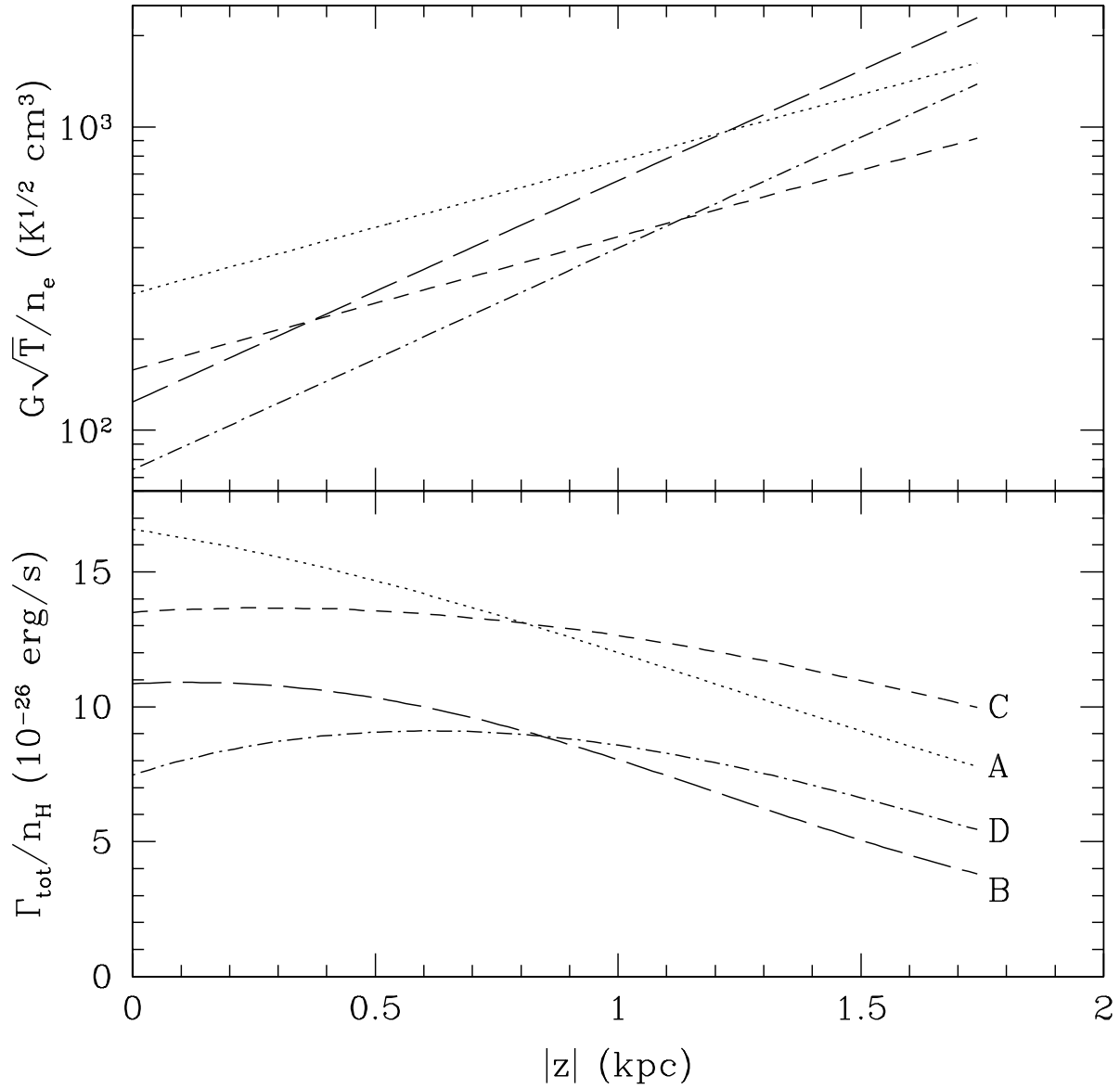


Fig. 22.— Upper panel: Values of the charging parameter as a function of  $|z|$  for the four cases of Table 7. Lower panel: The ratio of the net grain heating rate (i.e. photoelectric heating minus collisional cooling) to the gas density as a function of  $|z|$ , for the four cases of Table 7.

Table 1. Blackbody Components of the ISRF (Mathis et al. 1983)

$i$	$w_i$	$T_i/\text{K}$
1	$10^{-14}$	7500
2	$1.65 \times 10^{-13}$	4000
3	$4 \times 10^{-13}$	3000

Table 2. Grain Distribution Parameter Values for Extinction Fits<sup>a</sup>, Part 1

$R_V^b$	$f_g^c$	$\alpha_g$	$a_{t,g}$ ( $\mu\text{m}$ )	$\beta_g$	$a_{c,g}$ ( $\mu\text{m}$ )	$C_g$
3.1	0.0	−2.58	0.134	−3.56	0.860	$7.03 \times 10^{-14}$
3.1	0.03	−2.49	0.125	−3.62	0.917	$9.22 \times 10^{-14}$
3.1	0.05	−2.42	0.126	−3.72	1.05	$9.44 \times 10^{-14}$
3.1	0.07	−2.37	0.127	−3.74	0.961	$9.65 \times 10^{-14}$
3.1	0.1	−2.20	0.114	−3.78	1.00	$1.49 \times 10^{-13}$
4.0	0.0	−2.49	0.202	−4.01	1.55	$2.17 \times 10^{-14}$
4.0	0.03	−2.38	0.184	−3.88	1.21	$2.90 \times 10^{-14}$
4.0	0.05	−2.30	0.181	−3.95	1.46	$3.16 \times 10^{-14}$
4.0	0.07	−2.09	0.149	−3.88	1.51	$6.19 \times 10^{-14}$
4.0	0.1	−1.67	0.135	−4.15	2.24	$1.12 \times 10^{-13}$
5.5	0.0	−2.40	0.229	−2.71	0.632	$1.11 \times 10^{-14}$
5.5	0.03	−2.12	0.222	−4.10	2.47	$1.67 \times 10^{-14}$
5.5	0.05	−1.77	0.180	−3.93	1.99	$3.43 \times 10^{-14}$

<sup>a</sup>See equations (47) and (48).

<sup>b</sup> $R_V = A_V/E_{B-V}$ , ratio of visual extinction to reddening

<sup>c</sup>Fraction of the cosmic C in log-normal very small grain population (see equations 45 and 46)

Table 2. Grain Distribution Parameter Values for Extinction Fits, Part 2

$a_{\min,s}$ ( $\text{\AA}$ )	$\alpha_s$	$a_{t,s}$ ( $\mu\text{m}$ )	$\beta_s$	$a_{c,s}$ ( $\mu\text{m}$ )	$C_s$
38.9	−2.57	0.119	0.198	0.197	$1.57 \times 10^{-13}$
25.9	−2.54	0.120	0.098	0.198	$1.57 \times 10^{-13}$
15.6	−2.47	0.127	0.073	0.199	$1.49 \times 10^{-13}$
15.0	−2.51	0.116	−0.062	0.196	$1.75 \times 10^{-13}$
15.1	−2.53	0.116	−0.075	0.193	$1.71 \times 10^{-13}$
106.	−2.66	0.110	1.09	0.195	$1.02 \times 10^{-13}$
68.6	−2.55	0.105	0.573	0.202	$1.23 \times 10^{-13}$
59.8	−2.60	0.094	0.077	0.211	$1.54 \times 10^{-13}$
24.7	−2.50	0.089	−0.360	0.218	$1.86 \times 10^{-13}$
22.9	−2.61	0.090	0.252	0.186	$1.61 \times 10^{-13}$
271.	−2.71	0.083	0.462	0.229	$9.78 \times 10^{-14}$
199.	−2.43	0.081	0.454	0.221	$1.04 \times 10^{-13}$
85.5	−2.24	0.074	0.182	0.221	$1.28 \times 10^{-13}$

Table 2. Grain Distribution Parameter Values for Extinction Fits, Part 3

$\tilde{V}_g^d$	$\tilde{V}_s^d$	$\chi_1^{2e}$	$\chi_2^{2f}$
0.873	1.37	0.014	0.027
0.882	1.37	0.014	0.027
0.880	1.38	0.015	0.034
0.889	1.37	0.016	0.031
0.913	1.33	0.018	0.034
0.755	1.03	0.010	0.024
0.746	1.06	0.011	0.023
0.746	1.08	0.012	0.023
0.763	1.07	0.013	0.025
0.828	0.960	0.018	0.029
0.560	0.969	0.012	0.017
0.609	0.921	0.013	0.021
0.618	0.915	0.015	0.021

<sup>d</sup>Total grain volumes in the graphite (including the log-normal contribution) and silicate populations, normalized to their values for the MRN distribution ( $2.67 \times 10^{-27}$  and  $2.79 \times 10^{-27}$  cm<sup>3</sup>/H, respectively)

$${}^e\chi_1^2 = \sum_i (\ln A_{\text{obs}} - \ln A_{\text{mod}})^2 / \sigma_i^2.$$

$${}^f\chi_2^2 = \sum_i (\ln A_{\text{obs}} - \ln A_{\text{mod}})^2.$$

Table 3. Photoelectric Heating Parameters;<sup>a</sup> Part 1

$R_V$	$f_g$	rad field <sup>b</sup>	$C_0$	$C_1$	$C_2$	$C_3$
3.1	0.0	B0	5.42	0.003500	0.006610	0.008390
3.1	0.03	B0	5.69	0.003120	0.003380	0.013700
3.1	0.05	B0	5.92	0.002760	0.003190	0.013600
3.1	0.07	B0	7.03	0.000715	0.011100	0.003360
3.1	0.1	B0	7.46	0.003310	0.017100	0.004270
4.0	0.0	B0	3.58	0.001100	0.023000	0.001150
4.0	0.03	B0	3.23	0.000447	0.001420	0.005680
4.0	0.05	B0	4.38	0.000864	0.019700	0.000994
4.0	0.07	B0	4.20	0.008790	0.007580	0.006150
4.0	0.1	B0	4.69	0.000564	0.003950	0.004540
5.5	0.0	B0	1.56	0.000545	0.025100	0.001210
5.5	0.03	B0	1.80	0.029200	0.012600	0.002760
5.5	0.05	B0	2.08	0.000662	0.003210	0.003650
3.1	0.0	ISRF	4.71	0.003080	0.031400	0.008020
3.1	0.03	ISRF	5.13	0.001230	0.032300	0.001370
3.1	0.05	ISRF	4.13	0.006490	0.001020	0.002030
3.1	0.07	ISRF	6.05	0.009880	0.030800	0.000610
3.1	0.1	ISRF	4.50	0.000544	0.000625	0.002620

<sup>a</sup>See eq (51).

<sup>b</sup>B0 refers to a blackbody spectrum with  $T_c = 3 \times 10^4$  K and the ISRF of Mathis et al. (1983) is defined in eq (32).

Table 3. Photoelectric Heating Parameters, Part 2

$C_4$	$C_5$	$C_6$	err <sup>c</sup>	$h_s$ <sup>d</sup>
0.739	0.665	0.561	0.17	0.62
0.766	0.735	0.479	0.17	0.67
0.788	0.731	0.476	0.18	0.71
0.954	0.627	0.592	0.19	0.74
0.798	0.520	0.644	0.19	0.76
0.809	0.605	0.686	0.18	0.52
0.903	0.875	0.424	0.19	0.64
0.880	0.598	0.665	0.20	0.70
0.629	0.622	0.561	0.19	0.76
0.946	0.716	0.517	0.21	0.81
0.779	0.534	0.746	0.18	0.52
0.409	0.581	0.623	0.18	0.71
0.832	0.708	0.551	0.21	0.79
0.713	0.478	0.616	0.21	0.59
0.854	0.520	0.689	0.18	0.64
0.657	0.889	0.482	0.20	0.67
0.660	0.567	0.681	0.23	0.70
0.949	0.926	0.423	0.21	0.73

<sup>c</sup>Largest fractional error for  $10 \leq T \leq 10^4$  K and  $10^2 \leq G\sqrt{T}/n_e \leq 10^6$  K<sup>1/2</sup> cm<sup>3</sup>.

<sup>d</sup>Fraction of the total heating due to grains with  $a < 100$  Å, for  $G\sqrt{T}/n_e = 10^2$  K<sup>1/2</sup> cm<sup>3</sup> and  $T = 100$  K.

Table 4. Collisional Cooling Parameters<sup>a</sup>, Part 1

$R_V$	$f_g$	rad field <sup>b</sup>	$D_0$	$D_1$	$D_2$
3.1	0.0	B0	0.4259	2.387	-8.775
3.1	0.03	B0	0.4403	2.432	-8.633
3.1	0.05	B0	0.3169	3.202	-9.954
3.1	0.07	B0	0.4927	1.971	-7.313
3.1	0.1	B0	0.4846	2.149	-7.560
4.0	0.0	B0	0.4088	2.643	-10.220
4.0	0.03	B0	0.4188	2.456	-9.174
4.0	0.05	B0	0.5544	1.511	-6.776
4.0	0.07	B0	0.3447	3.079	-9.963
4.0	0.1	B0	0.4684	2.085	-7.272
5.5	0.0	B0	0.3941	2.681	-11.186
5.5	0.03	B0	0.4335	2.393	-9.430
5.5	0.05	B0	0.4175	2.421	-8.959
3.1	0.0	ISRF	0.5262	2.001	-7.217
3.1	0.03	ISRF	0.4612	2.579	-7.735
3.1	0.05	ISRF	0.4496	2.544	-7.128
3.1	0.07	ISRF	0.4132	2.922	-7.967
3.1	0.1	ISRF	0.3915	2.946	-7.679

<sup>a</sup>See eq (52).

<sup>b</sup>B0 refers to a blackbody spectrum with  $T_c = 3 \times 10^4$  K and the ISRF of Mathis et al. (1983) is defined in eq (32).

Table 4. Collisional Cooling Parameters, Part 2

$D_3$	$D_4$	err
1.847	0.06828	0.15
1.806	0.06548	0.14
2.099	0.07623	0.16
1.616	0.05779	0.14
1.641	0.05774	0.14
1.957	0.07188	0.16
1.837	0.06661	0.12
1.389	0.04782	0.16
2.016	0.07189	0.13
1.556	0.05310	0.13
2.008	0.07405	0.15
1.758	0.06201	0.12
1.741	0.06100	0.13
1.459	0.05126	0.15
1.552	0.05299	0.12
1.482	0.05007	0.13
1.643	0.05616	0.11
1.642	0.05581	0.12

Table 5. Photoelectric Heating Rates for H II Regions

$R_V^d$	$f_g^e$	$T_c^f$	$G/n_H =$	$\Gamma_{pe}/Gn_H^{a,b}$			$\Gamma_{pe}/Gn_H^{a,c}$		
				0.1 <sup>g</sup>	1.0	10.	0.1	1.0	10.
3.1	0.0	3.5		0.97	0.82	0.45	4.0	3.5	1.8
3.1	0.1	3.5		1.3	1.2	0.71	5.9	5.3	3.1
4.0	0.0	3.5		0.51	0.43	0.25	2.2	1.9	1.0
4.0	0.1	3.5		0.91	0.82	0.53	4.3	3.9	2.4
5.5	0.0	3.5		0.23	0.20	0.12	1.0	0.87	0.47
5.5	0.05	3.5		0.39	0.36	0.25	2.0	1.8	1.1
3.1	0.0	4.5		1.1	0.91	0.49	7.0	5.9	2.7
3.1	0.1	4.5		1.5	1.3	0.78	9.9	8.7	4.6
4.0	0.0	4.5		0.57	0.48	0.27	3.5	2.9	1.4
4.0	0.1	4.5		1.0	0.91	0.59	7.3	6.5	3.6
5.5	0.0	4.5		0.25	0.22	0.13	1.6	1.3	0.63
5.5	0.05	4.5		0.44	0.40	0.27	3.3	3.0	1.6

<sup>a</sup> $10^{-25}$  erg s<sup>-1</sup>

<sup>b</sup>Blackbody spectrum cut off at 13.6 eV

<sup>c</sup>Full blackbody spectrum

<sup>d</sup> $R_V = A_V/E_{B-V}$ , ratio of visual extinction to reddening

<sup>e</sup>Fraction of the cosmic C in log-normal very small grain population  
(see equations 45 and 46)

<sup>f</sup> $10^4$  K

<sup>g</sup>Value for  $G/n_H$ , in cm<sup>3</sup>

Table 6. Recombination Cooling Rates for H II Regions

$R_V^d$	$f_g^e$	$T_c^f$	$G/n_H =$	$\Lambda/Gn_H^{a,b}$			$\Lambda/Gn_H^{a,c}$		
				0.1 <sup>g</sup>	1.0	10.	0.1	1.0	10.
3.1	0.0	3.5		12.	1.5	0.29	13.	1.9	0.49
3.1	0.1	3.5		28.	3.2	0.52	29.	3.8	0.85
4.0	0.0	3.5		6.3	0.77	0.14	6.5	1.0	0.26
4.0	0.1	3.5		23.	2.5	0.39	24.	3.0	0.65
5.5	0.0	3.5		2.8	0.34	0.066	3.0	0.45	0.12
5.5	0.05	3.5		11.	1.2	0.18	11.	1.4	0.30
3.1	0.0	4.5		12.	1.5	0.30	13.	2.3	0.62
3.1	0.1	4.5		28.	3.2	0.53	29.	4.2	1.1
4.0	0.0	4.5		6.3	0.78	0.15	6.7	1.1	0.31
4.0	0.1	4.5		23.	2.6	0.40	24.	3.3	0.81
5.5	0.0	4.5		2.8	0.35	0.069	3.0	0.51	0.14
5.5	0.05	4.5		11.	1.2	0.18	11.	1.5	0.37

<sup>a</sup> $10^{-25}$  erg s<sup>-1</sup>

<sup>b</sup>Blackbody spectrum cut off at 13.6 eV

<sup>c</sup>Full blackbody spectrum

<sup>d</sup> $R_V = A_V/E_{B-V}$ , ratio of visual extinction to reddening

<sup>e</sup>Fraction of the cosmic C in log-normal very small grain population  
(see equations 45 and 46)

<sup>f</sup> $10^4$  K

<sup>g</sup>Value for  $G/n_H$ , in cm<sup>3</sup>

Table 7. WIM Heating Examples

Case	Grain Size Distribution	WIM Filling Factor	G
A	$R_V = 3.1, f_g = 0.0$	0.2	0.8
B	$R_V = 3.1, f_g = 0.0$	$0.1 \exp  z /750 \text{ pc}$	0.5
C	$R_V = 3.1, f_g = 0.1$	0.2	0.45
D	$R_V = 3.1, f_g = 0.1$	$0.1 \exp  z /750 \text{ pc}$	0.3